ornl

OAK RIDGE NATIONAL LABORATORY

LOCKHEED MARTIN

MANAGED AND OPERATED BY
LOCKHEED MARTIN ENERGY RESEARCH CORPORATION
FOR THE UNITED STATES
DEPARTMENT OF ENERGY

ORNL-27 (3-96)

ORNL/TM-12972

FY 1995 Progress Report on the ANS Thermal-Hydraulic Test Loop Operation and Results

M. Siman-Tov
D. K. Felde
G. Farquharson
J. L. McDuffee
M. T. McFee
A. E. Ruggles
M. W. Wendel
G. L. Yoder

Originated: September 30, 1995
Published: July 1997

ANS
Advanced Neutron Source

ORNL/TM-12972

FY 1995 PROGRESS REPORT ON THE ANS THERMAL-HYDRAULIC TEST LOOP OPERATION AND RESULTS

M. Siman-Tov
D. K. Felde
G. Farquharson
J. L. McDuffee
M. T. McFee
A. E. Ruggles
M. W. Wendel
G. L. Yoder

Originated: September 30, 1995
Published: July 1997

Prepared by
OAK RIDGE NATIONAL LABORATORY
Oak Ridge, Tennessee 37831-6285
managed by
LOCKHEED MARTIN ENERGY RESEARCH CORP.
for the
U.S. DEPARTMENT OF ENERGY
under contract DE-AC05-96OR22464

CONTENTS

LIST OF FIGURES

LIST OF TABLES

ACRONYMS

ANS	Advanced Neutron Source
ANSR	Advanced Neutron Source Reactor
BPR	bypass ratio
CHF	critical heat flux
DNB	departure from nucleate boiling
FE	flow excursion
IB	incipient boiling
LOCA	loss-of-coolant accident
OFI	onset of flow instability
ONVG	onset of net vapor generation
ORNL	Oak Ridge National Laboratory
OSV	onset of significant void
S&Z	Saha and Zuber
T/C	thermocouple
T/H	thermal-hydraulic
THTL	Thermal-Hydraulic Test Loop
W&F	Whittle and Forgan

NOMENCLATURE

A	=	cross section area (m^2)
b	=	flow channel gap (m)
C	=	a constant [Eq. 24]
C_p	=	mean coolant specific heat (kJ/kg·K)
D_h	=	hydraulic diameter (m)
E	=	electric voltage to test section (kV)
f	=	friction factor
G	=	mass flux ($kg/m^2 \cdot s$)
h	=	heat transfer coefficient ($W/m^2 \cdot k$)
I	=	electric current to test section (A)
k	=	thermal conductivity (kW/m·K)
L	=	heated length (m)
Nu	=	Nusselt Number (-) = $\frac{q D_h}{k \Delta T_{sub}}$
P	=	pressure (Pa)
Pe	=	Peclet Number (-) = $\frac{G C_p D_h}{k}$
P_h	=	heated perimeter (m)
R	=	electrical resistance (Ω)
Q	=	heat rate (kW)
q	=	heat flux (kW/m^2)
St	=	Stanton Number (-) = $\frac{q}{G C_p \Delta T_{sub}}$
T	=	temperature (K)
t	=	thickness (m)
V	=	coolant velocity (m/s)
x	=	distance along channel (m)
n	=	exponential constant [Eq. 22]
ΔP	=	pressure drop (Pa)
ΔT	=	temperature difference (K)
ρ	=	coolant density (kg/m^3)
η_{sub}	=	subcooling correction factor

Subscripts

acc	=	acceleration
al	=	aluminum
av	=	average across and along the test section
b	=	bulk coolant
c	=	value at the minimum ΔP point
cal	=	calculated
cool	=	coolant
cs	=	cross section of the flow
dem	=	demand side

fe	=	at the flow excursion point
fr	=	friction
ele	=	electrical
ex	=	exit of channel
ext	=	external
gen	=	generated
gr	=	gravity
h	=	heated
in	=	inside
loc	=	local
loss	=	heat losses from test section
m	=	measured
out	=	at channel outlet
ox	=	oxide film layer
red	=	spanwise heat redistribution
s	=	saturated
sub	=	subcooling value (T_s - T_b)
tot	=	total
ts	=	test section
w	=	wall
xs	=	cross section of the aluminum

ABSTRACT

The Thermal-Hydraulic Test Loop (THTL) is an experimental facility constructed to support the development of the Advanced Neutron Source Reactor (ANSR) at Oak Ridge National Laboratory (ORNL). The ANSR was intended to become the world's highest-flux steady-state thermal neutron source for scientific experiments. The average and peak heat fluxes in the reactor are 5.9 and 12 MW/m^2, respectively, with a nominal total thermal power of 300 MW. Highly subcooled heavy-water coolant (1.7 MPa and 84°C at the exit) flows vertically upward at a very high mass flux of 25 Mg/m^2s. In a parallel fuel plate configuration as in the ANSR, the flow is subject to a potential excursive static-flow instability that can very rapidly lead to flow starvation and departure from nucleate boiling (DNB) in the "hot channel." The existing correlations and experimental data bases for flow excursion (FE) and critical heat flux (CHF) seldom extend to the specific combination of ANSR operating parameters.

The THTL facility was designed and built to provide known thermal-hydraulic (T/H) conditions for a simulated full-length coolant subchannel of the ANS reactor core, thus facilitating experimental determination of FE and CHF thermal limits under expected ANSR T/H conditions. Special consideration was given to allow operation of the system in a "stiff" mode (constant flow) and in a "soft" mode (constant pressure drop) for proper implementation of true FE and DNB experiments. The facility is also designed to examine other T/H phenomena, including onset of incipient boiling (IB), single-phase heat transfer coefficients and friction factors, and two-phase heat transfer and pressure drop characteristics. Tests will also be conducted that are representative of decay heat levels at both high pressure and low pressure as well as other quasi-equilibrium conditions encountered during transient scenarios.

A total of 22 FE tests and 2 CHF tests were performed during FY 1994 and FY 1995 with water flowing vertically upward. These tests in combination with earlier tests covered a very wide parametric range that includes a nominal heat flux range of 0.7 to 18 MW/m^2; a mass flux range of 2.7 to 28 Mg/m^2s; exit pressures of 0.17, 0.4, and 1.7 MPa; and an inlet temperature range of 40 to 50°C. Some FE experiments were conducted using as "soft" a system as possible to secure a true FE phenomena (actual secondary burnout). True DNB experiments under similar conditions were conducted using a "stiff" system. Eight of these FE tests and one CHF test were performed with a wider span to determine the scalability of the channel span. To the authors' knowledge, no other FE data have been reported in the literature to date that cover such a combination of conditions of high mass flux, high heat flux, and moderately high pressure.

Comparison of these data as well as extensive data from other investigators led to a proposed modification to the Saha and Zuber correlation for onset of significant void (OSV), applied to FE prediction. The modification takes into account a demonstrated dependence of the OSV or FE thermal limits on subcooling levels, especially in the low subcooling regime.

1. INTRODUCTION

The Thermal-Hydraulic Test Loop (THTL) is an experimental facility constructed to support the development of the Advanced Neutron Source Reactor (ANSR) at Oak Ridge National Laboratory (ORNL). The Advanced Neutron Source (ANS) is a state-of-the-art research reactor facility designed to become the world's most advanced thermal neutron flux source for scientific experiments. Therefore, the core of the ANSR must accommodate very high power densities using very high coolant mass flux and subcooling levels. Statistical/probabilistic uncertainty analysis was performed to determine the optimal design power and to provide the necessary safety margin. This analysis requires selecting the most appropriate thermal-hydraulic (T/H) correlations and developing uncertainty distribution profiles based on the best available data.

The ANSR is cooled and moderated by heavy water and uses highly enriched uranium silicide fuel. The core is composed of two concentric annular core halves, each shifted axially and radially with respect to the other (see Fig. 1). There are 684 parallel aluminum-clad fuel plates (252 comprise the inner-lower core and 432 comprise the outer-upper core). Each plate is 1.27–mm thick and is arranged in an involute geometry that effectively creates an array of thin, rectangular flow channels. The coolant channels have a 1.27-mm gap width, spans of 87 and 70 mm (lower and upper core, respectively), and a 507-mm heated length. Each fuel plate has 10 mm of unheated leading and trailing edges, with all the channels having common inlet and outlet plenums with nominal pressures of 3.2 and 1.7 MPa, respectively. The coolant flows vertically upward at an inlet velocity of 25 m/s and a Reynolds number of 99,000. The inlet and average outlet temperatures are 45 and 85°C, respectively. The average heat flux is 5.9 MW/m^2 with a radial and axial maximum of 12 MW/m^2. A more complete description of the ANSR configuration and T/H conditions is given by Yoder et al. (1993).

The ANSR core configuration with many parallel channels is subject to a potential static instability called flow excursion (FE), which differs from a true critical heat flux (CHF) that would occur at a fixed channel flow rate, as discussed later. The existing correlations and experimental data bases for FE and CHF seldom cover the specific combination of ANSR operating parameters. This observation is reflected in Boyd's excellent survey on subcooled flow boiling CHF (Boyd 1985) and for FE in Duffey and Hughes (1990); Lee, Dorra, and Bankoff (1992); and Rogers and Li (1992). In addition, many investigators in the past did not distinguish between FE and true CHF, which adds to the inconsistencies in the available FE and CHF data bases, since both are very complex but different phenomena. The general process of correlation evaluation and selection, as well as the correlations currently used in the ANSR T/H analysis, are discussed by Siman-Tov et al. (1991).

A THTL facility was designed and built to provide a simulated full-length coolant subchannel of the ANS reactor core, to enable experimental determination of FE and CHF thermal limits under expected ANSR T/H conditions. Determination of these two thermal limits and the relationship between them is the main objective of the THTL facility. However, the facility is also designed to examine other T/H phenomena, including onset of incipient boiling (IB), single-phase heat transfer coefficients and friction factors, and two-phase heat transfer and pressure drop characteristics.

Although the facility's primary aim is to investigate thermal limits at the ANSR nominal conditions for normal operation and safety margin analysis, tests will also be conducted that are representative of decay heat levels at both high pressure (e.g., loss of off-site power) and low pressure [e.g., a loss-of-coolant accident (LOCA)] as well as other quasi-steady-state conditions encountered during transient scenarios. This report will discuss the 1994 and 1995 experiments focused on the FE phenomena at ANS nominal conditions and the few true CHF experiments performed for comparison. A condensed version of the material presented in this report was published by Siman-Tov et al. (1993, March 1995, and April 1995). The reader should also refer to an earlier progress report (Siman-Tov et al. 1994) and for a general description of the THTL facility, to Felde et al. (1994).

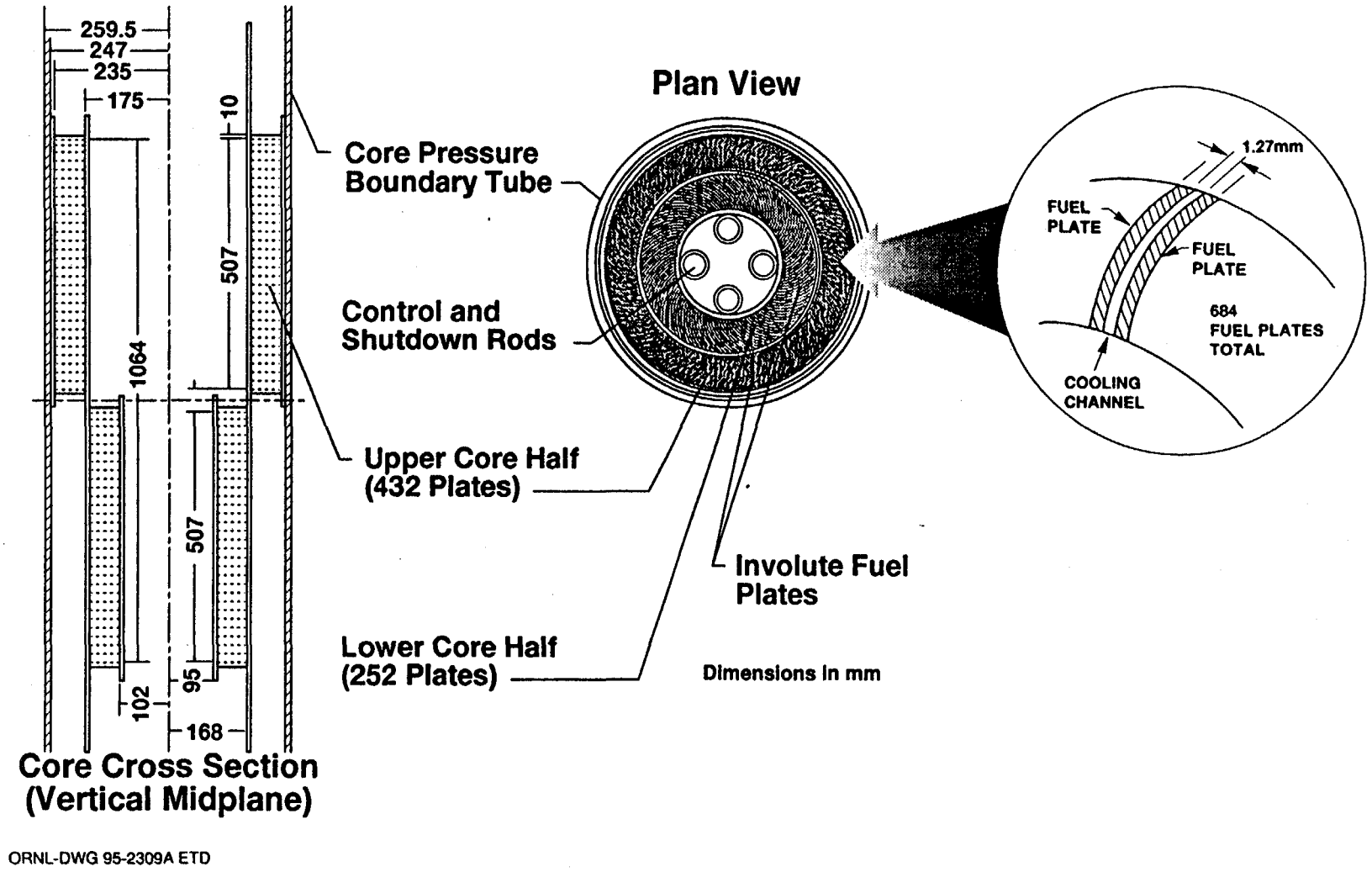

Fig. 1. ANSR core assembly and fuel plates arrangement.

2. THE NATURE OF THE ADVANCED NEUTRON SOURCE REACTOR THERMAL LIMITS

The cooling channels in the ANSR fuel assembly are all parallel and share common inlet and outlet plenums, effectively imposing a common pressure drop across all the channels. This core configuration is subject to FE and/or flow instability (Leddineg 1938, 1949) that may occur once boiling is initiated in any one of the channels. The FE phenomenon constitutes a different thermal limit than a true CHF or departure from nucleate boiling (DNB). In such a system, initiation of boiling in one of the channels (i.e., the hot channel) can result in flow redistribution to the other, cooler channels. This process can very rapidly lead to flow starvation, which, in turn, leads to a DNB in the hot channel at flows lower than the nominal flow rate. The FE phenomenon is in contrast to a primary DNB that occurs at a nominally constant flow rate, referred to here as a "true CHF."

The more complete way to predict the occurrence of FE is to perform flow vs pressure drop analysis of the parallel channels involved and predict the subsequent flow redistribution under constant and common pressure drop boundary conditions. Performing this prediction is quite complex because of the uncertainties involved in predicting void fractions and pressure drops in two-phase flow. In reality, after boiling starts, the flow resistance of the channel increases, leading to flow reduction in the channel. The flow reduction promotes more boiling, which, after a certain point, rapidly leads to a more severe flow starvation. Therefore, it is nominally accepted that FE [also referred to as the onset of flow instability (OFI)] will most likely occur near the point where sustained net vapor first appears. This point is called the onset of net vapor generation (ONVG) point (Costa 1967) or the point of onset of significant void (OSV).

Maulbetsch and Griffith (1965) and other investigators analytically and experimentally demonstrated the conditions under which excursive instability will occur. They determined that such instability will occur "if the slope of the (demand) pressure drop vs flow rate (or velocity) is more negative than that of the external supply system." This statement is expressed mathematically as (Maulbetsch and Griffith 1965):

$$\frac{d(\Delta P_{ext})}{dV} > \frac{d(\Delta P_{ts})}{dV} \quad . \tag{1}$$

Figure 2 presents a typical plot of the pressure drop vs flow rate relationship under various boundary conditions. In the case of many parallel channels between large common headers, as is the case in the ANSR, the pressure-drop slope of the external supply system is practically zero and is represented in Fig. 2 by horizontal lines (A and B). Based on this observation, FE or OFI conditions were determined in most of the THTL FE experiments by detection of the test section pressure-drop minimum as the flow to the test section was reduced under a constant heat flux. This method allowed for repetition of many nondestructive FE tests without experiencing an actual FE that normally causes test section failure. For confirmation and comparison, limited experiments were performed with an actual FE burnout, and some experiments were run with true CHF burnout under constant flow. To accommodate these experiments, the design of the THTL system had to respond to three separate modes of operation, as enumerated below.

1. A **"soft"** system was used to perform actual FE tests with burnout. In this mode, a large bypass around the test section was fully open so that the flow could split between the test section and the bypass to maintain an almost constant common pressure drop across both, thus closely simulating the ANSR configuration.
2. A **"stiff"** system was used to perform true CHF tests with actual burnout at constant and known flow rates. In this mode, the bypass around the test section was completely closed to maintain a constant flow through the test section. In addition, a near-positive displacement pump that provides a nearly constant flow rate was used in the primary loop. This pump is insensitive to the system pressure-drop characteristics. Small-

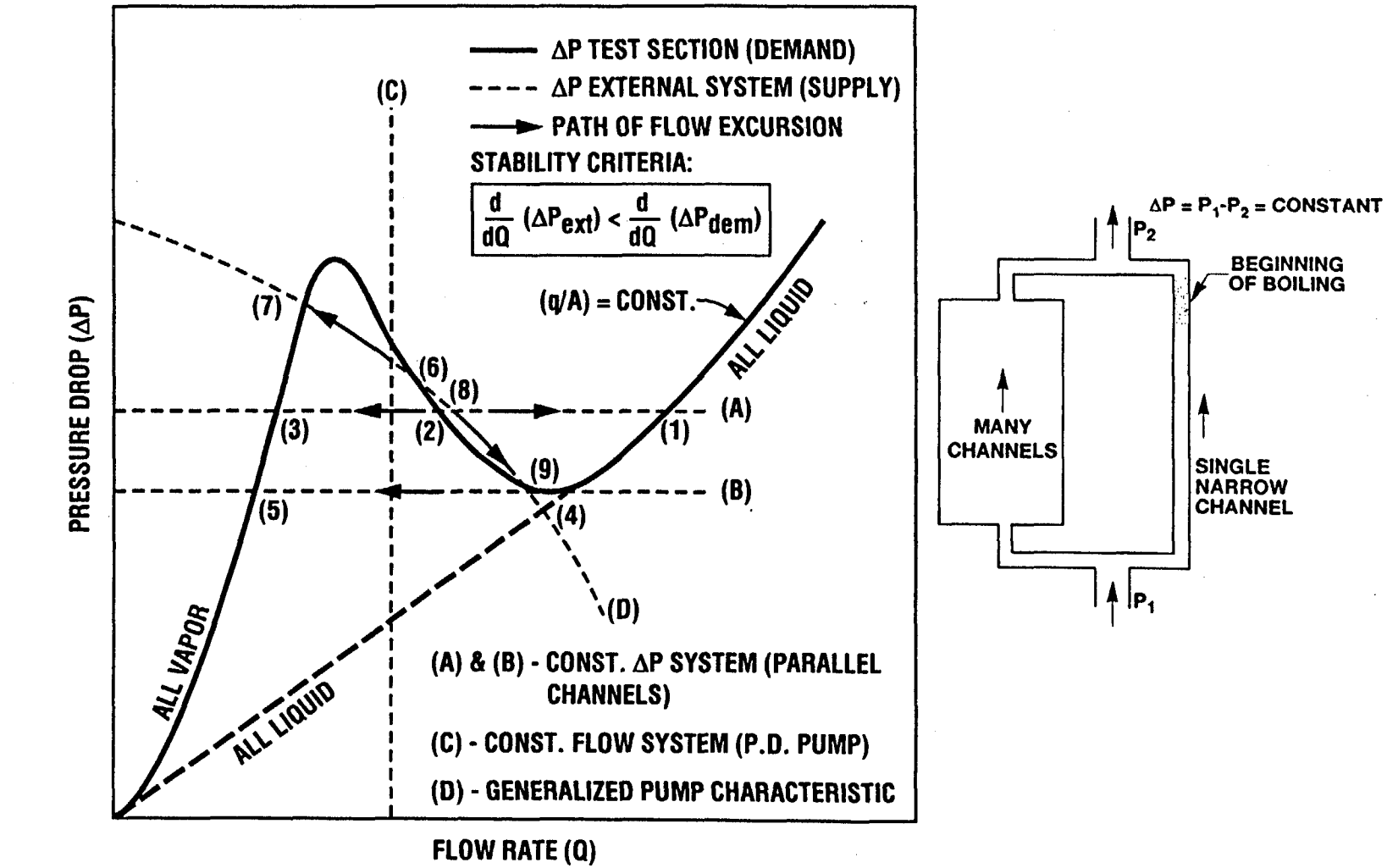

ORNL-DWG 93M-2658A4

Fig. 2. Phenomena and criteria leading to FE instability.

diameter piping (to reduce volume) and a throttling valve were also used upstream of the test section inlet to enhance flow stability.

3. A **modified "stiff"** system was used to perform simulated FE tests without experiencing actual FE. In this mode, a closed or minimal bypass configuration, along with a significant pressure drop across the flow control valve upstream of the test section, was used to prevent actual FE or other flow instability. In this case, the potential for FE was determined by detecting the minimum pressure drop in a plot of pressure drop vs flow rate (which coincides with the ONVG point), as demonstrated by Maulbetsch and Griffith (1965), Whittle and Forgan (1967), Costa (1967), Johnston (1988), Dougherty et al. (1989), and others. Most of the FE tests were performed using this approach.

Since the ANSR has many channels in parallel, an ideal bypass simulation in the THTL "soft" system would require a very large bypass flow ratio ("infinite bypass") and therefore an unrealistically large pump. In practice, however, a reasonable but not ideal flow ratio can provide a very close simulation with no significant error. The lowest bypass flow ratio necessary, which still provides sufficiently constant pressure-drop boundary conditions, was investigated in two independent studies—one transient and one steady-state as discussed by Siman-Tov et al. (1994)

Knowing which of the two types of limiting phenomena—true CHF or FE—should be used as a thermal limit for the ANSR configuration is crucial. In most cases, FE will precede true CHF in such a configuration (Waters 1966). However, the sequence of these phenomena depends on the specific conditions involved. It was demonstrated that FE will occur at heat fluxes much lower than the CHF (as low as half) at low pressure, low velocities, and low subcooling (Maulbetsch and Griffith 1965). It is noteworthy, however, that the margin between FE and CHF narrows as the level of these parameters increases, and, at a certain point, the trend may even reverse (Boyd 1988). Since ANSR normally operates at moderate pressures and very high mass flux and subcooling levels, one of the main goals of these tests is to determine the relationship between CHF and FE under ANSR conditions.

Another critical question for the ANSR design is the application of either FE or true CHF to local fuel plate conditions, such as "hot spots" and "hot streaks," that may occur on the fuel plate over a small, limited area as a result of manufacturing imperfections that cause local heat flux peaking. In addition, the effect of the hot subchannel* on these thermal limits must be addressed. Because experimental evidence indicates little mixing across the span (Costa 1967, Waters 1966, Yan and Theofanous 1992), FE in a hot subchannel can be treated as a narrow, independent subchannel in relation to the rest of the flow in the rectangular channel. Therefore, the heat flux and subcooling in each one of these subchannels can be applied independently, just as in the parallel channel configuration. The present ANSR T/H design technique applies appropriate uncertainties to each location on the fuel plate and checks the resulting heat flux against various limiting criteria, including FE and CHF. Since it is recognized that very localized boiling will not sufficiently impact the channel pressure drop to cause FE, FE is not used as a limiting criterion when the region of the fuel plate causing the limiting conditions is below a predetermined size (Yoder et al. 1993).

---

*A "hot subchannel" is defined here as an axial region of a certain width along the fuel plate that yields a maximum bulk coolant temperature rise. This region is also occasionally referred to as a "hot stripe."

3. FACILITY DESCRIPTION

The THTL was designed and built to provide a simulated full-length coolant subchannel of the ANS reactor core, allowing experimental determination of the thermal limits (both FE and CHF) under anticipated ANS T/H conditions. An isometric view of the facility is shown in Fig. 3, and a schematic diagram of the loop and its major components and instrumentation is presented in Fig. 4. A detailed description of the test facility is given by Felde, Yoder, and Skrzycke (1992) and by Felde et al. (1994). In the design process, special consideration was given to include the proper pump, test section bypass configuration, and system valving and piping to allow operation of the system in either stiff or soft modes, as discussed earlier.

The Moyno primary circulation pump is driven by a variable-speed motor through a gear drive. This pump and motor combination is capable of providing a wide range of flow and pressure conditions with near-positive displacement characteristics, which means that flow supply is insensitive to the loop pressure drop. Using the variable speed of the motor drive provides the capability for operating over most of the pump flow-pressure drop diagram up to 2.5×10^{-3} m^3/s flow and 4.1 MPa differential pressure across the pump at 750 rpm. When this pump is used in combination with the test section bypass line, a very wide range of mass flow conditions at the test section is possible. In the stiff mode, with a closed bypass, a near-constant test section mass flux in the range of 7 to 42 Mg/m^2s can be used. (The maximum mass flux is limited by the overall pressure rating for the test loop.) In the soft mode, with a bypass flow ratio of 10 to 1, a maximum mass flux of 12 Mg/m^2s at a near-constant bypass pressure drop can be used. At a 5 to 1 bypass flow ratio, this maximum increases to 23 Mg/m^2s. The approximation of the ideal bypass ratio (infinite) with a practical bypass ratio is in the nonconservative direction for FE data, but, as discussed earlier, it is believed that the approximation is sufficient from a practical point of view.

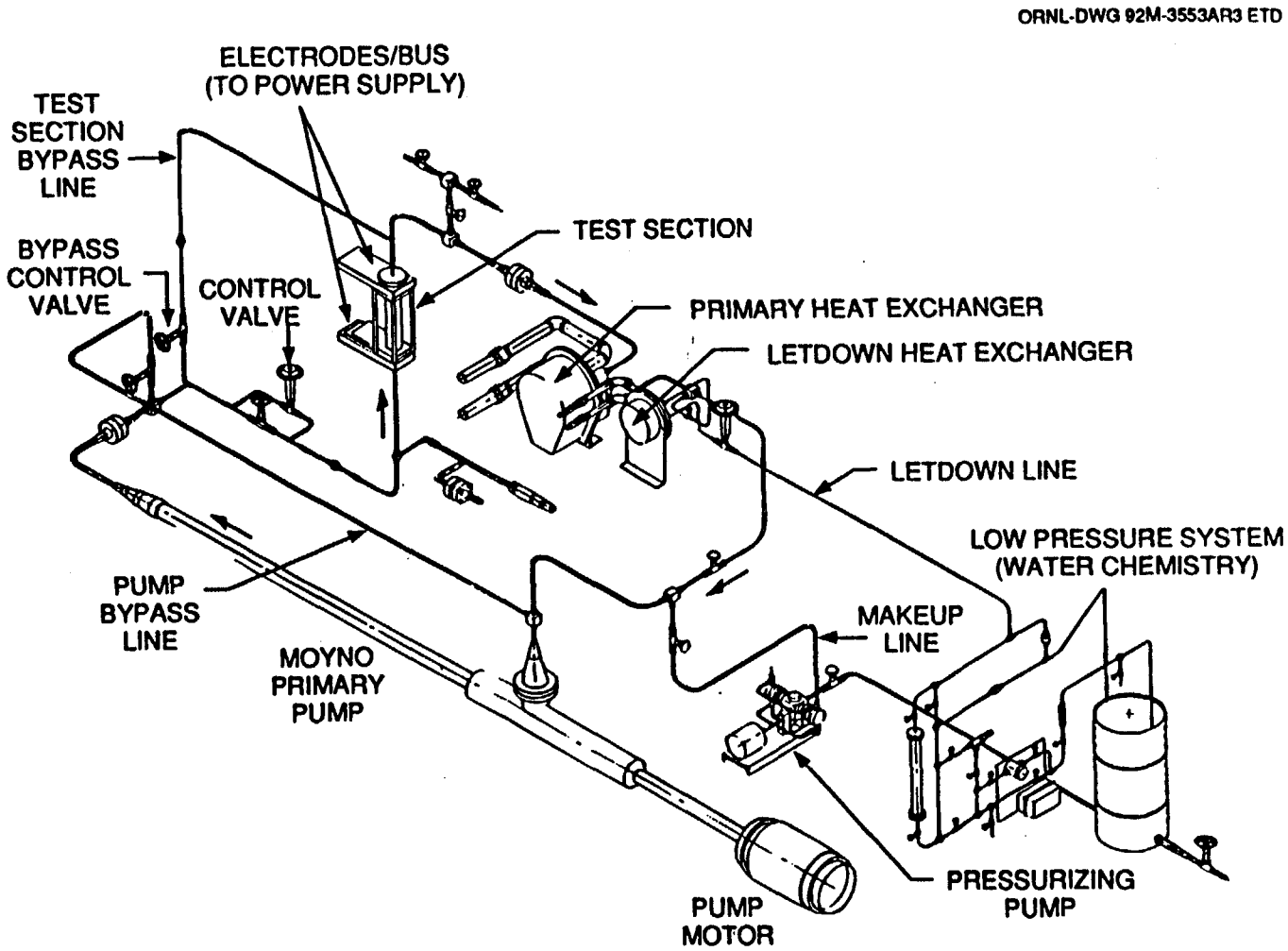

Fig. 3. Advanced Neutron Source (ANS) Thermal-Hydraulic Test Loop (THTL).

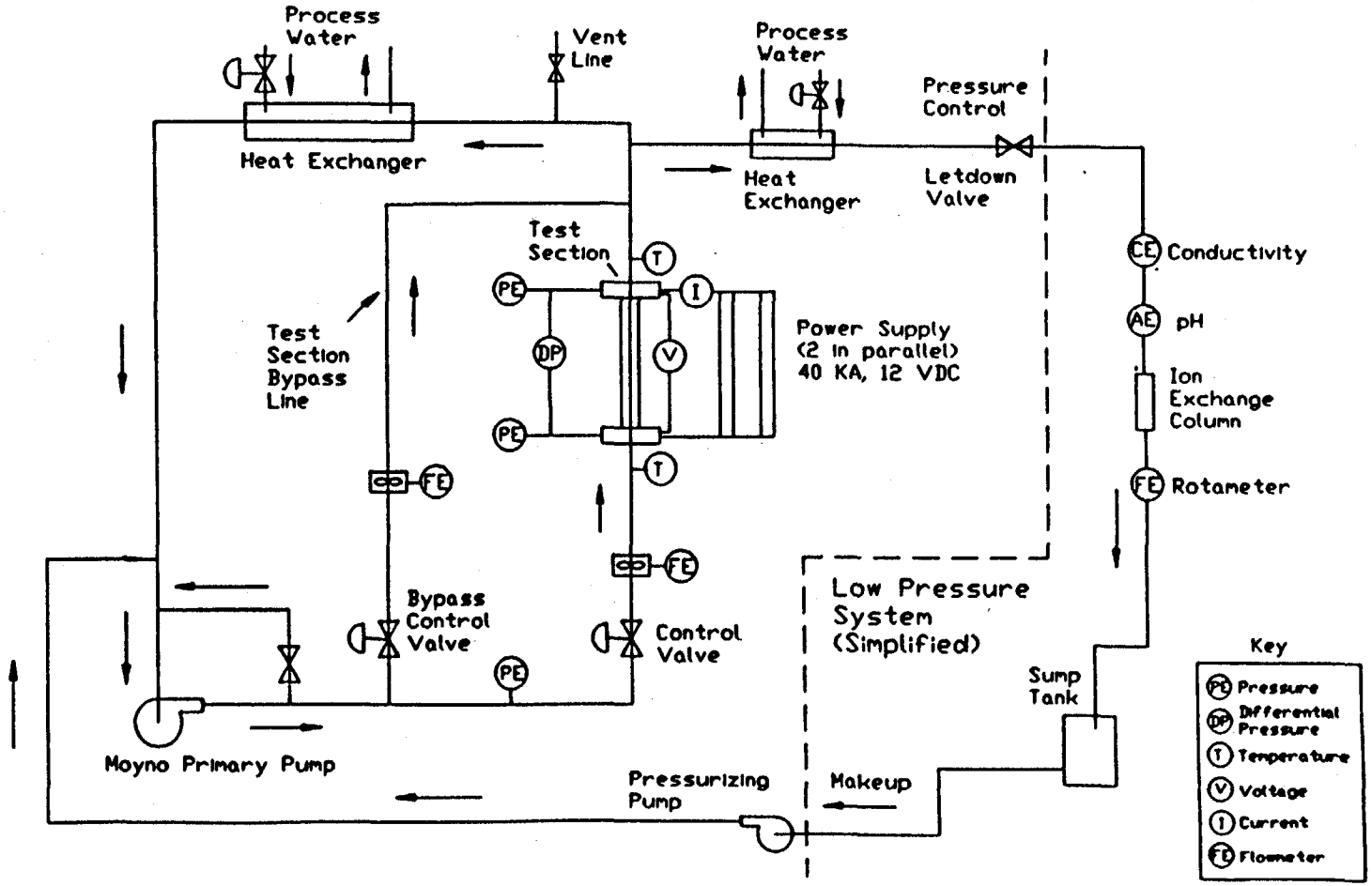

Fig. 4. Schematic diagram of the THTL primary components and instrumentation.

4. TEST CHANNEL DESIGN

The test section and its boundary conditions were of primary interest in determining the T/H limits. A detailed description of the test channel design is given by Felde, Yoder, and Skrzycke (1992) and by Felde et al. (1994). The cross-section design, shown in Fig. 5, was similar to that used by Gambill and Bundy (1964) but was redesigned in accordance with the ANS characteristics. The test section simulated a single subchannel in the ANS reactor core with a cross section that had a full prototypic heated length (507 mm), the same flow-channel gap (1.27 mm), and the same material (aluminum) with a surface roughness (~0.5 μm) reasonably close to that expected in the ANSR fuel plates. Most of the tests were conducted with the channel span scaled down to 12.7 mm (vs 87 and 70 mm for core halves in the ANSR) to limit total power requirements to the test section. The involute shape of the plates was not simulated to simplify the experimental design and operation. Other researchers have demonstrated that there is little lateral fluid mixing in such rectangular channels, even under two-phase flow conditions (Costa 1967, Waters 1966, Yan and Theofanous 1992). Furthermore, sources also maintain that span width (or span-to-gap ratio) does not have a significant effect on either CHF or FE within certain limits (Whittle and Forgan 1967 and Gambill and Bundy 1964). Several tests were conducted with a wider span test channel design of 25.4 mm in order to address scaling issues. The wider span design was identical to the cross section shown in Fig. 5 with the exception of the 2.7-mm span dimension. The test section wall thickness was 2.54 mm, dictated by the voltage/current of the power supplies. The reduced wall thickness at the curved ends was designed to reduce the heat flux and prevent the coolant bulk temperature from peaking on the curved ends of the channel, which could have led to premature burnout. The ratio of heat flux on the curved ends to that on the flat ends was 36% for the design shown in Fig. 5. Possible effects of lateral and axial heat redistribution by thermal conduction within the test section metal will be considered later through the use of a 3-D conduction model (see Sects. 6.2 and 6.3).

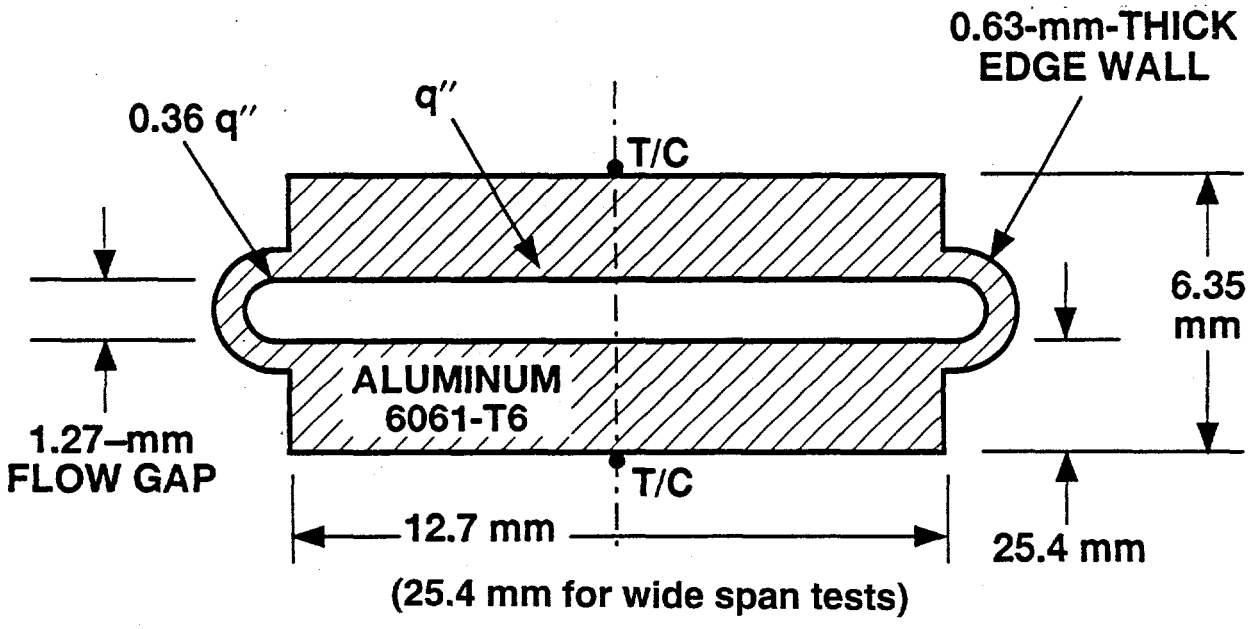

Fig. 5. Cross section of the channel in the THTL.

The test channel was instrumented on the back of the channel wall with type N thermocouples (T/Cs). The locations of these thermocouples on the test section are shown in Fig. 6. The spacing was staggered, as shown, to provide improved definition in the region close to the channel's exit, where FE or CHF was expected. Measurements at the center span were made on both sides of the channel at each axial location for redundancy. Additional instrumentation shown in Fig. 6 was added during this period to provide an improved method for determining the axial heat flux distribution. These measurements are made using the common mode voltage present on the spring-loaded ribbon-type thermocouples installed along the back wall of the test channel and provide a measurement of the voltage drop between each thermocouple location. Transmitters were installed to continuously measure this differential voltage between each of the thermocouples. Pressure and temperature of the water were measured at the test section inlet and outlet with the pressure taps installed in the test section flanges, as shown in Fig. 6. The taps were located axially 12.7 mm from the "heated" channel at each end, which allowed a closer determination of the pressure drop across the heated region, minimizing the effects of possible condensation and dynamic pressure recovery that can occur between the end of the heated channel and the point of pressure measurement (Costa 1967).

The test channel was enclosed inside a stainless steel pressure backing and was thermally and electrically isolated from the backing by Mycalex insulation. The test channel was either welded or brazed on both ends into aluminum flanges, each 2.54 cm thick. The test section flanges were sandwiched between two 2.54–cm thick aluminum electrical bus plates. The water connection to the test section was made concentrically inside this bus connection by a 5.08–cm flange and Teflon gasket that were fastened through the test section flange. The Teflon gasket and Micarta bolt sleeves provide electrical isolation for the piping loop. The stainless steel backing, which was in direct contact with the test section flanges at both ends, was split in the center and isolated at this point by Mycalex insulation. This design effectively separated the electrical contact requirements from the water sealing requirements of the loop interface.

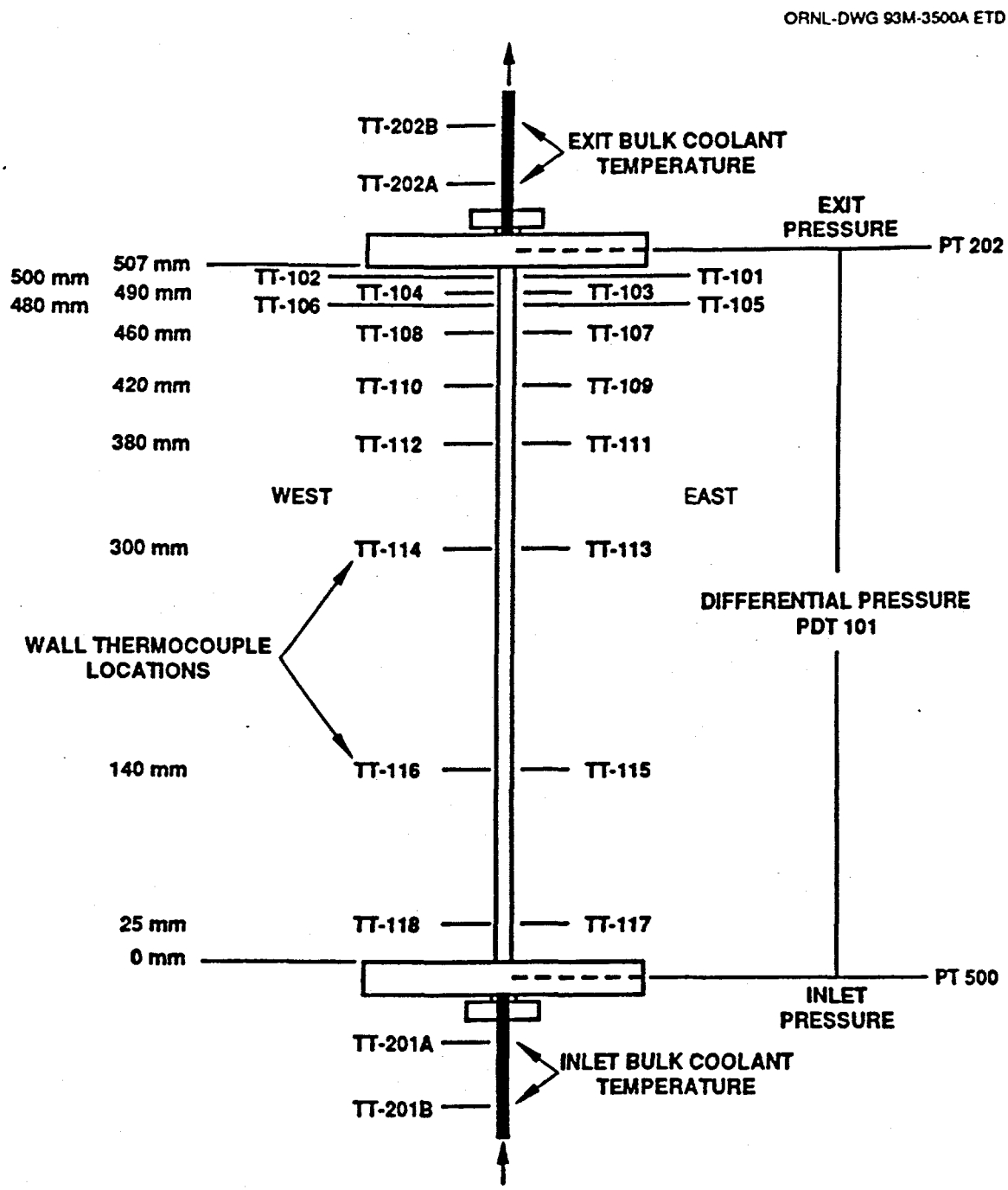

Fig. 6. THTL test section instrumentation.

5. EXPERIMENTAL PROCEDURES

A detailed description of the experimental procedures and operation is given by Felde, Yoder, and Skrzycke (1992) and by Felde et al. (1994). Prior to installation of the test channel assembly into the loop, the channel surface undergoes a surface treatment procedure similar to that used for fuel elements in the High Flux Isotope Reactor at ORNL and expected to be used for the ANSR fuel elements. This procedure involves cleaning and degreasing, followed by an acid treatment and hot water rinse. In addition, the as-fabricated flow channel gap is measured at locations along the axial length using a capacitance-type probe inserted into the channel. These data are used to improve conversion of volumetric flow measurements (made upstream from the test section) to local velocities in the channel.

Flow excursion tests (without burnout) are conducted in a stiff mode, as described earlier. These tests are initiated by controlling test section flow to a level where no boiling exists at the target heat flux level. The applied power to the test section is then raised to produce the target heat flux level. Exit pressure is automatically controlled via the system letdown valve and high-pressure makeup pump at the desired setting (nominally, 1.7 MPa). Process water flow to the secondary side of the heat exchanger is also automatically controlled to maintain the inlet bulk coolant temperature at the desired set point (nominally, 45°C).

Data are recorded continuously during these processes by the personal computer-based data acquisition system. Once the system is stabilized and data are obtained under steady-state conditions, the velocity is reduced to a lower level while monitoring the measured differential pressure across the test channel. This reduction is made through either pump speed reduction, flow control valve positioning, bypass flow adjustment, or some combination of the above, depending on the proximity of the conditions to the expected minimum. As the minimum is approached, the loop configuration is adjusted to minimize the amount of bypass flow and to maximize the pressure drop across the control valve to prevent an actual excursion and channel failure. The system is allowed to stabilize at each of the selected velocity settings. Power supply and velocity adjustments are made concurrently to maintain the average heat flux constant. (This concurrent adjustment is necessary because the temperature coefficient of resistivity of the aluminum affects the current-voltage characteristics of the test channel as velocity is reduced and test channel wall temperatures increase.) Once the minimum in pressure drop has been clearly determined (by observation of increasing pressure drop as velocity is further decreased), the velocity is increased once again, and data are taken for comparison at some of the velocity points obtained during the earlier sequence.

6. DATA REDUCTION AND ANALYSIS

A number of data reduction models and analysis methods were developed to facilitate design of certain features of the experimental loop, planning the tests, analyzing the data acquired, interpreting the results, and comparing the results with existing correlations. Those were discussed in the previous progress report (Siman-Tov et al., 1994). The most important of these is the THTL data reduction code that is discussed in the following sections.

6.1 PROGRAM FUNCTIONS

The THTL data reduction code is used to coordinate, plan, and evaluate the results of thermal-hydraulic tests conducted at the THTL facility. The THTL data reduction program was originally written in Quick Basic (Siman-Tov et al, 1994), but was recently converted to Visual Basic to take advantage of the greater flexibility and graphics capabilities. This program is a steady-state, 1-D code that evaluates the flow and heat transfer characteristics of the coolant in the channel in addition to a 1-D conduction/generation calculation in the aluminum walls. Sections 6.1.1 through 6.1.4 describe the various capabilities of the THTL data reduction program. A complete listing of the program language in Visual Basic, tabulated lists and definitions of all its input, measured and calculated parameters, and its logical block diagram are provided in Appendix A.

6.1.1 Steady-State Analysis

This function provides a detailed picture of the test section at a particular point in time. The available data points are chosen in advance as being representative of the situation at that time, usually because that particular point contained the median value of pressure drop for that specific velocity. The program allows various types of calculational procedures to be chosen including options regarding the calculation of heat loss (Sect. 6.3.1), heat redistribution (Sect. 6.3.2), and oxide thicknesses (Sect. 6.4.5), as shown in Fig. 7. The resulting analysis gives details on virtually every aspect of the thermal-hydraulic condition of the test section, both globally and locally (see list in Sect. 6.2), and includes graphs of the temperature profile, heat transfer coefficient, heat flux, and pressure drop, as shown in Figs. 8 and 9.

6.1.2 Transient Graphics

This function is designed to show the general thermal-hydraulic trends for an entire run (usually several hours worth of data). There are standard graphs available that show temperature, power, pressure, and velocity profiles as a function of time so that an overall picture of the test's data can be analyzed, as shown in Fig. 10. In addition, any two measured variables may be plotted against one another. This is often used in flow excursion runs by plotting the measured pressure drop against the coolant inlet velocity, thereby finding the velocity that corresponds to the minimum pressure drop as shown in Fig. 11.

6.1.3 THTL Predictor

This utility is used primarily during preparation for an experimental run. The predictor takes a set of global and inlet parameters (inlet velocity, test section geometry, average heat flux, etc.) and calculates local quantities throughout the test section. It will also vary the velocity or heat flux in order to find the conditions that bring about IB, FE, or CHF conditions at a particular thermocouple location, as shown in Fig. 12. This information is very useful when preparing for a test and ensures that the minimum in the demand curve is reasonably close to that expected by the design team.

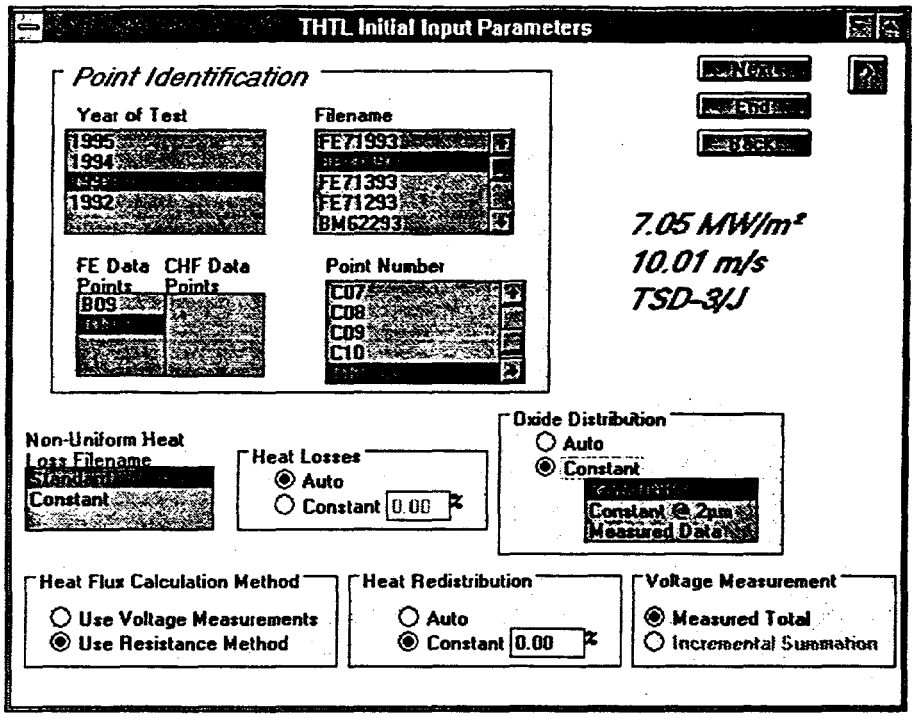

Fig. 7. Steady-state analysis parameter input screen.

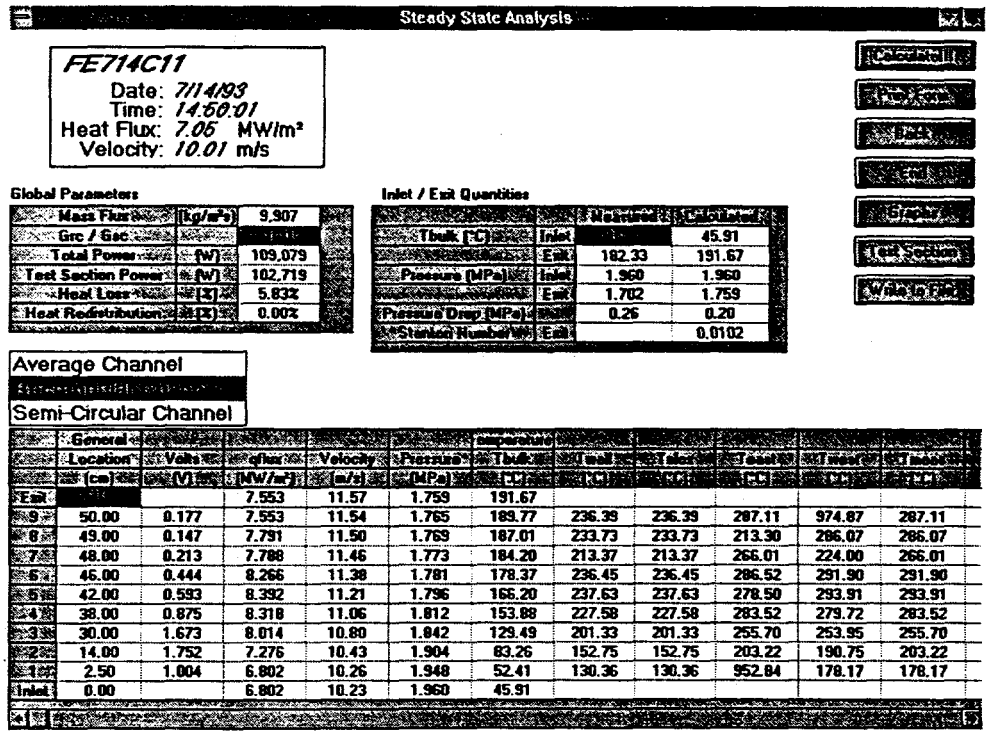

Fig. 8. Steady-state analysis results.

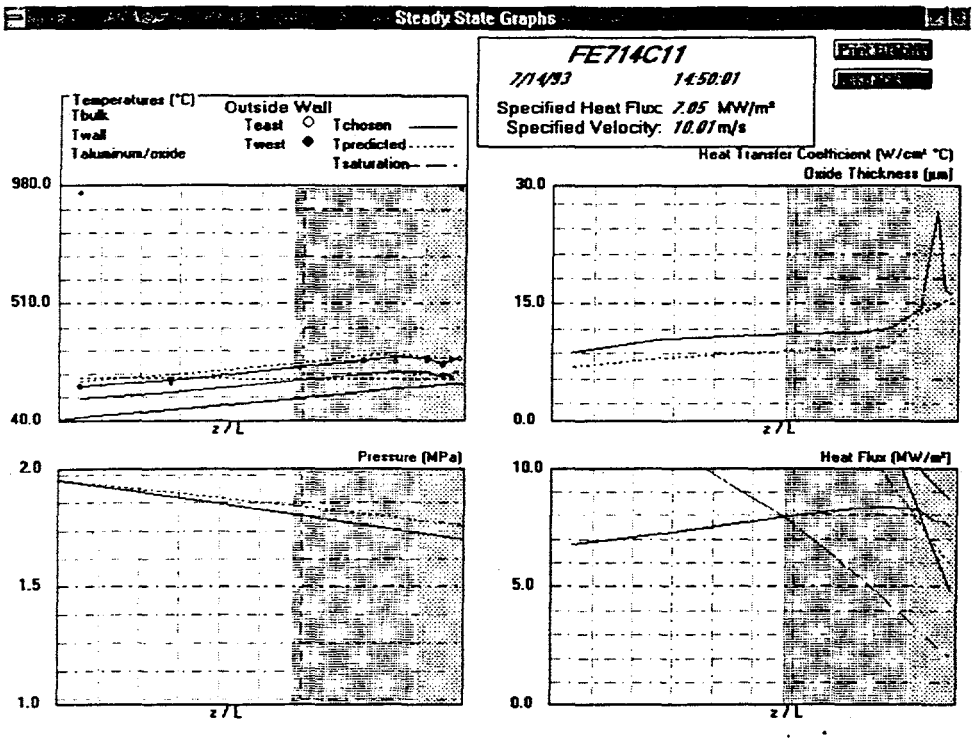

Fig. 9. Steady-state analysis graphs.

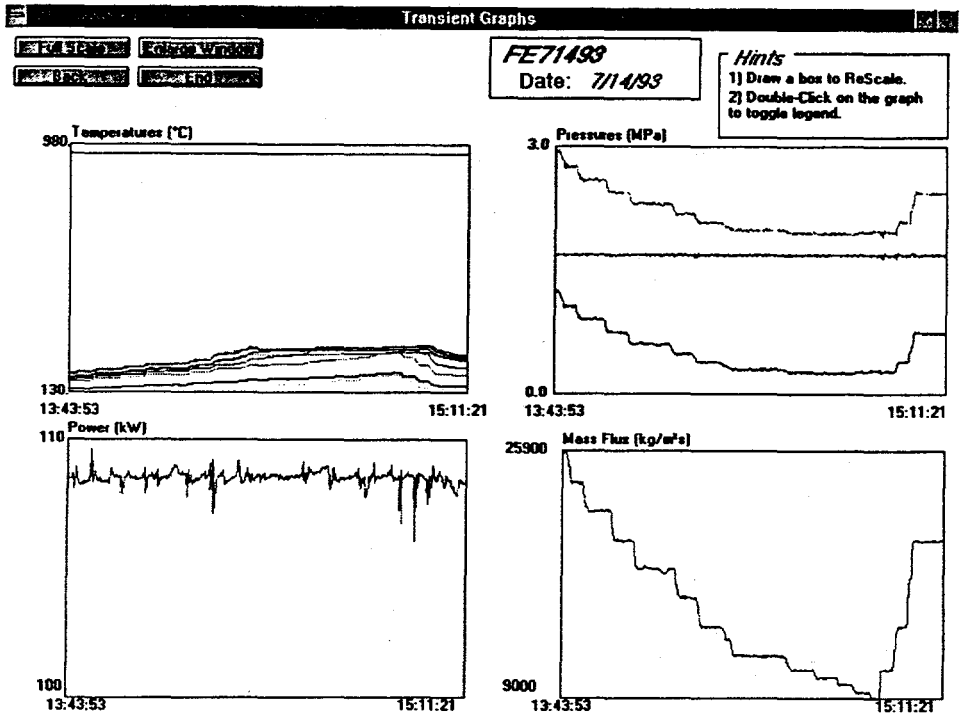

Fig. 10. Standard transient graphic.

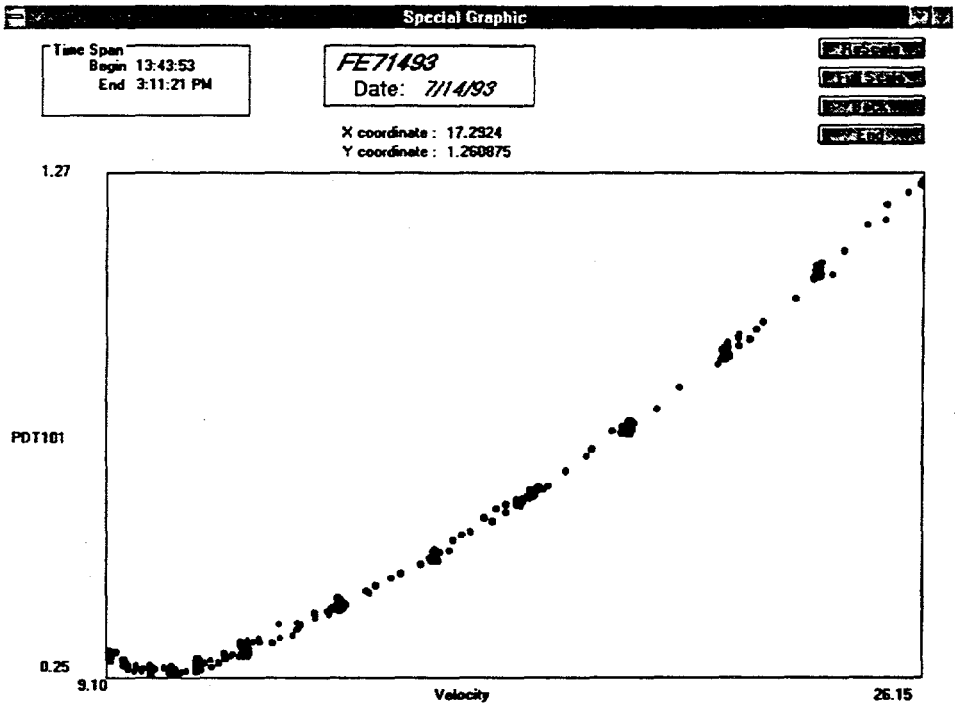

Fig. 11. Special transient graphic.

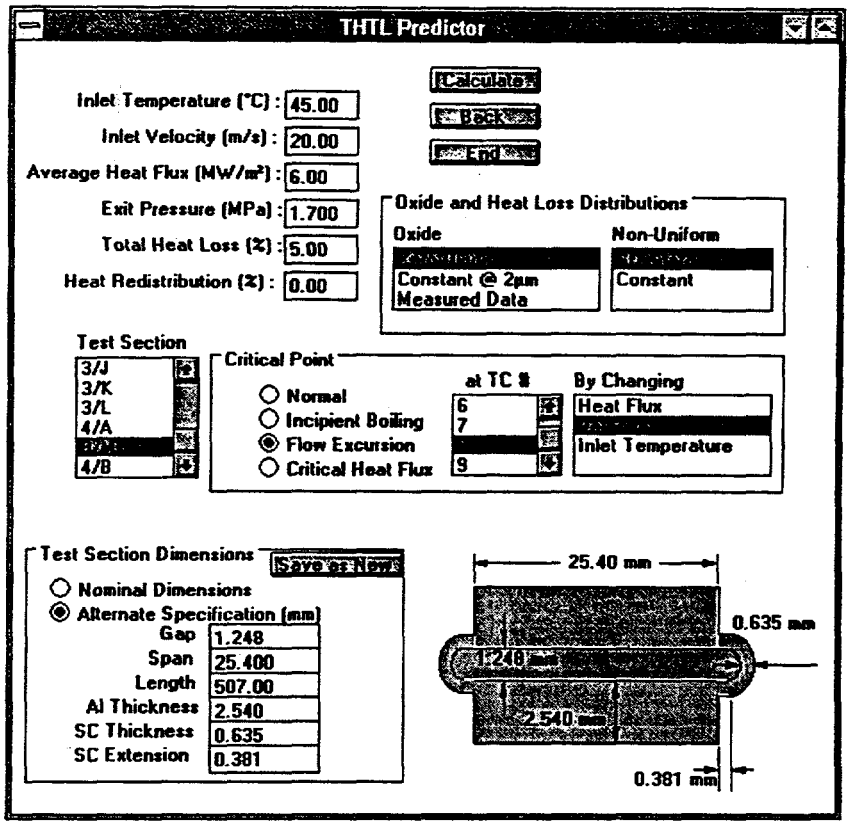

Fig. 12. THTL predictor input screen.

6.1.4 Evaluation of THTL Uncertainties

The multitude of calculations necessary to find estimates of the implicitly determined local variables (heat flux, bulk temperature, wall temperature, etc.) makes the determination of experimental uncertainties problematic. Standard methods such as Propagation Of Error become so analytically complicated that they become impossible to solve. In addition, there is no real analytical method for determining the uncertainty involved in estimating the heat redistribution fraction (Sect. 6.3.2) or the local oxide thicknesses (Sect. 6.4.5).

Because of these problems, a Monte Carlo uncertainty utility was added to the THTL data reduction program to estimate these uncertainties through random sampling. In this method, a normal distribution is introduced to all measured variables, including test section dimensions. Most of the standard deviations used for these analyses were provided by the manufacturers of the instruments. The mean for each variable is assumed to be the measured value of the present data point.

For the uncertainty analysis a particular data point is chosen, usually representing an FE minimum or CHF point. The measured data at that point are adjusted randomly within their normal distribution. This new data set is then analyzed in a manner identical to that described in Sect. 6.1.1, and the results of interest, usually the exit heat flux and Stanton number, are stored in a separate file. The measured data are then again adjusted randomly, and the process is repeated. This sequence will be repeated hundreds or perhaps thousands of times until there is little change in the standard deviations of the results. In this way, the uncertainties of the important test results can be determined from the uncertainties in the measured data.

Preliminary uncertainty analyses show that the standard deviation associated with the resulting Stanton number at the FE minimum is about 11%. These analyses also show that less than 2% of this variance is due to random fluctuations in time, indicating that the manufacturer's uncertainty estimates are conservative.

6.2 MEASURED AND CALCULATED VARIABLES

The raw data collected by the THTL facility is originally stored in a direct-access, comma-delimited file with each column representing a measured datum (temperature, voltage, etc.) and each row representing a data set for a particular time. Before analysis with the THTL program, this file is converted to a random access file with each data set stored in a record named Rawdata. The Rawdata record is given in Table A.1 in Appendix A, which lists the variable name, number of array elements, and a brief description of each field in the record. Note that some of the fields are arrays and contain several quantities. The measured outside wall temperature array, for example, is an array containing 18 elements, each representing either the east or west side of the test section at one of the nine axial locations (see Fig. 6).

More general information is stored externally to the program in two comma-delimited files. The file "thtldata.csv" stores the test section dimensions for each test section used in the THTL facility. The file "datapts.csv" stores information about the data points of interest for each of the data files taken at the THTL facility.

The THTL program uses several internally defined variables to aid in calculation of the desired parameters. Most of these variables are arranged and stored in records that serve to associate variables of similar function. Table A.2 in Appendix A lists these variables.

6.3 GLOBAL CALCULATIONS

Some of the basic parameters of interest, such as average heat flux and heat losses to the atmosphere, can be determined from global measurements. These global parameters also serve as the basis of the initial guesses made for bulk temperatures, wall temperatures, and other local parameters that require iteration.

6.3.1 Average Heat Flux and Total Heat Loss

The total heat lost to the atmosphere is calculated by first finding the total power generated.

$$Q_{gen} = IE \quad . \tag{2}$$

where I is the current and E is the voltage drop in the test section. The total heat loss is found by comparing the heat generated in the test section to the bulk enthalpy rise in the coolant flow.

The definition of Q_{loss} also serves to provide the heat loss fraction,

$$Q_{loss} = 1 - \frac{GA_{cs}\, C_p\, (T_{ex}-T_{in})}{Q_{gen}} \quad , \tag{3}$$

$$\alpha_{loss} = \frac{Q_{loss}}{Q_{gen}} \quad , \tag{4}$$

and the average heat flux for the test section:

$$q_{av} = \frac{Q_{gen}-Q_{loss}}{P_h L} = \frac{Q_{gen}(1-\alpha_{loss})}{P_h L} \quad . \tag{5}$$

6.3.2 Heat Redistribution

The purpose of the heat redistribution parameter is to consider the heat lost from the spanwise centerline of the test section. As shown in the lower part of Fig. 13 and discussed in Sect. 6.4.3, the THTL data reduction calculations assume l-D heat flow from the outside wall to the coolant flow. Unfortunately, the experimental results so far obtained indicate that a significant fraction (5–15%) of the heat flow distributes itself spanwise as shown in the upper portion of Fig. 13. This is due to less heat generation (see Fig. 13) and cooler temperatures in the semicircular section, as well as the high thermal conductivity of the aluminum. If the heat redistribution is not properly taken into account, the best estimates of the internal wall temperature and heat transfer coefficient are in serious disagreement with accepted correlations. The Petukhov heat transfer coefficient, for example, is known to be accurate within 10%, but is consistently 10–50% low when compared to the THTL best estimate if heat redistribution and oxide film buildup are not properly taken into account.

The THTL data reduction model provides an estimate of the heat redistribution fraction based on the following assumptions.

1. The Petukhov heat transfer coefficient correlation is an accurate predictor under THTL conditions. This assumption was verified by a previous report.
2. The heat redistribution profile is linear with axial distance and zero at the inlet.

A weighted average of the ratio of the measured-to-predicted heat transfer coefficient is made for the test section to obtain the average heat redistribution. The local heat redistribution is a linear function with a value of zero at the test section inlet and twice the average at the exit.

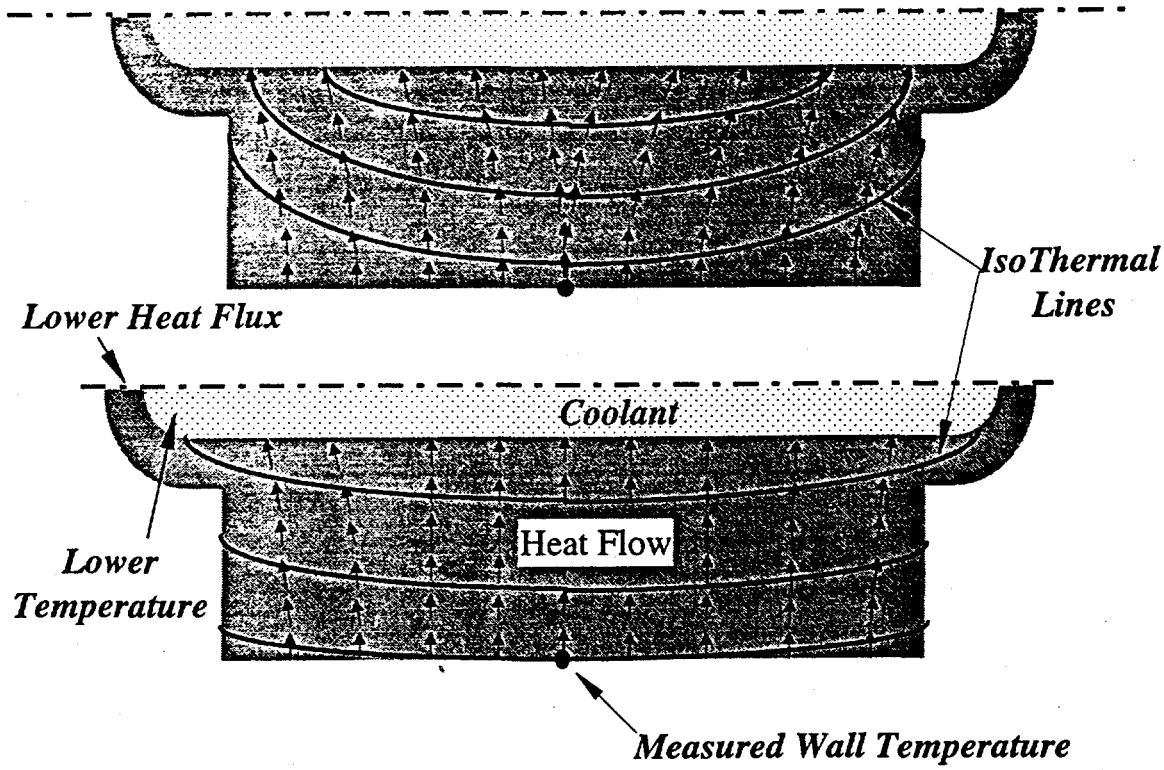

Fig. 13. Schematic of test section heat flow distribution.

Although the heat redistribution fraction, α_{red}, and the heat loss fraction, α_{loss}, are treated similarly, there is a fundamental difference between them that should be noted. The heat loss fraction represents heat that escapes to the atmosphere and never reaches the coolant flow. The heat redistribution fraction represents heat that is removed from the centerplane of the test section span in the rectangular portion of the cross section. This redistributed heat is not lost but is rather added to the coolant at a slightly different location. The bulk temperature profile is not affected by the amount of redistributed heat.

6.4 LOCAL CALCULATIONS

The local heat flux, heat transfer coefficient, wall temperatures, and bulk temperatures are all implicit calculations, therefore an iterative scheme is used as a solution method. The equations listed in the following sections are solved repeatedly until convergence is reached. The convergence criteria is that all local heat fluxes in the jth iteration must agree within 0.01% with the local heat fluxes in the (j-l) iteration.

6.4.1 Local Power

There are two methods for calculating the local generated power. The older method uses a temperature dependent correlation for electrical resistivity in the aluminum wall to find the locally generated power. In late 1994, local voltage drop measurements were added to the THTL facility so that the local power could be calculated without the aid of a correlation. The present THTL data reduction program allows either method to be used if the voltage measurements are available.

When the local voltages are not measured or used, the resistance method is used to find the local power. The electrical resistivity of the aluminum test section is calculated based on an empirical curve fit.

$$\rho_d = 10^{-8}(3.9+0.011T_d) \quad . \tag{6}$$

The local resistance of each axial section, I, is therefore

$$R_i = \frac{\rho_d L_i}{A_{xs}} \quad . \tag{7}$$

In order to maximize the use of measured quantities, the local generated power is calculated based on the total applied power and the ratio of the local resistance to the total test section resistance.

$$Q_i = IV_i = I\left(V\frac{R_i}{\Sigma R_i}\right) \quad . \tag{8}$$

When the local voltage measurements are available, the resistivity calculation becomes unnecessary. The local generated power is simply

$$Q_i = I \quad V_i \tag{9}$$

6.4.2 Local Heat Flux

Once the local power is obtained, the local heat flux for each of the cross sectional sections (average, rectangular, semicircular) can be found based on the local heat loss factor α_{loss}, the heat redistribution factor, α_{red}, and geometrical considerations. The average heat flux over the entire cross sectional area is simply

$$q_{av,i} = \frac{Q_i(1-\alpha_{loss})}{P_{h,av}L} \quad . \tag{10}$$

The rectangular and semicircular sections of the cross sectional area can be considered parallel paths with respect to the electrical flow, so that the current in each section is determined by the ratio of that section's area to the total area. The local heat flux to these sections is therefore

$$q_{rc} = \frac{Q_i(1-\alpha_{loss})\frac{A_{rc}}{A_{cs}}}{P_{h,rc}L_i} \quad . \tag{11}$$

Note that q_{rc} is the heat flux applied in the rectangular section that serves to increase the bulk fluid enthalpy. The span-wise centerline heat flux, which is used to calculate the wall temperature and heat transfer coefficient as described in Sect. 6.3.2, must also account for the redistribution of heat.

$$q_{rc,mid} = \frac{Q_i(1-\alpha_{loss})(1-\alpha_{red})\frac{A_{rc}}{A_{cs}}}{P_{h,rc}L_i} \quad . \tag{12}$$

6.4.3 Temperatures

A 1-D conduction model through the aluminum wall with internal heat generation is used to calculate the temperature at the aluminum/oxide interface based on the measured temperature on the exterior of the test section wall (see Fig. 5). Since the thermal conductivity of aluminum is dependent on the aluminum temperature, the average aluminum temperature must also be calculated.

$$T_{av,al} = T_{al\text{-}ox,i} + \frac{q_{rc,mid,i} t}{3k_{av}} \quad , \tag{13}$$

where

$$T_{al\text{-}ox,i} = T_m - \frac{q_{rc,mid,i} t}{2k_{av}} \tag{14}$$

and

$$k_{av} = 156.93 + 0.18738\ T_{av,al} - 0.00025238\ T_{av,al}^2 \quad . \tag{15}$$

$T_{al\text{-}ox,i}$ is the temperature at the aluminum/oxide interface.

The temperature at the wall/fluid interface is modeled with a 1-D conduction calculation through the oxide layer.

$$T_{wall,i} = T_{al\text{-}ox,i} - \frac{q_{rc,mid,i}\ t_{ox}}{k_{ox}} \quad , \tag{16}$$

where the conductivity of the oxide is assumed to be 2.25 W/m°C.

The bulk temperature increase in an axial segment is calculated using the locally applied heat flux and a segment average value for specific heat. The resulting equations are solved iteratively.

$$T_{b,i} = T_{b,i-1} + \frac{q_i P_h L_i}{G\ A_{cs} C_p} \quad , \tag{17}$$

where L_i is the segment length, A_{cs} is the flow cross section, and G is the mass flux.

The predicted heat transfer coefficient is calculated using the Petukhov correlation with the Filonenko correlation for the Darcy friction factor. The measured heat transfer coefficient is calculated using the best estimate values for heat flux, wall temperature and bulk temperature.

$$h_{m,i} = \frac{q_i}{T_{w,i,} - T_{b,i}} \quad . \tag{18}$$

6.4.4 Pressure

One of the boundary conditions in the THTL data reduction program is that the local axial pressure must be constant across the span. Therefore, it is assumed that the semicircular section has a slightly lower mass flux than the average, while the rectangular section has a slightly higher mass flux than the average. This correction factor is found iteratively by ensuring that the exit pressure predicted for the rectangular section matches within 0.1% that of the semicircular section.

The pressure drop in the channel is composed of gravitational, frictional, and convective acceleration components. The acceleration component is due to the decreasing density of the coolant flow as the temperature increases in the channel.

$$P_{ex,i} = P_{in,i} - \Delta P_f - \Delta P_{acc} - \Delta P_g$$

$$= P_{in,i} - \frac{f L_i}{d} \frac{G^2}{2\rho_i} - G^2 \left[\frac{1}{\rho_{ex}} - \frac{1}{\rho_{in}} \right] - \rho_i g \quad . \tag{19}$$

The Filonenko correlation is used to calculate the friction factor, f.

Before September 1992, the pressure in the THTL facility was measured in an inlet pipe before the channel cross section was reduced to the 1.27-mm gap in the main channel. For these cases, a further form loss is introduced in the entrance reduction and exit enlargement sections so that the length over which the pressure drop is predicted and measured is compatible. Beyond September 1992, the pressure taps were placed in the inlet and exit flanges where the gap was equivalent to the main channel.

6.4.5 Oxide Thickness

In the original THTL data reduction program, the oxide thickness was assumed to be 2 μm for the entire test section. Later versions incorporated the ability to change the oxide thickness locally, and the present version will change the oxide thickness automatically to force the best estimate of the heat transfer coefficient toward that predicted by the Petukhov correlation (see also Sect. 6.3.2).

$$T_{w,i} = T_{cl-ox,i} - \frac{q_{rc,mid,i} \; t_{ox,i}}{k_{ox}} = T_{b,i} + \frac{q_{rc,mid,i}}{h_{coil,i}} \quad . \tag{20}$$

$$t_{ox,i} = \frac{k_{ox}(T_{cl-ox,i} - T_{b,i})}{q_{rc,mid,i}} - \frac{k_{ox}}{h_{coil,i}} \quad . \tag{21}$$

7. SCOPE OF TESTS PERFORMED

The current THTL (Figs. 3 and 4) and test section designs (Figs. 5 and 6) are the result of a number of initial shakedown and benchmark tests, which led to successive modifications in both the loop and the test section design. Initial emphasis was placed on the FE phenomena at nominal conditions. The first goal was to proceed from low levels of heat flux and velocity and then extend the tests to the extremely high levels required by the ANSR operating conditions. A total of 22 FE tests and 2 CHF tests were completed during FY 1994 and 1995. The FE experiments completed so far are within the following T/H conditions:

- coolant: light water, upward flow
- inlet coolant temperature: 45 °C (some at 40 °C)
- exit coolant pressure: 1.7 MPa (some at 0.45 and 0.17 MPa)
- local (exit) heat flux range: 0.7–18 MW/m^2
- corresponding exit velocity range: 2.8–28.4 m/s
- channel configuration (Figs. 5 and 6): rectangular 1.27 × (12.7 and 25.4) × 507 mm

Table 1 provides a summary of all the tests performed so far, including those of FY 1994 and FY 1995, with the key features indicated for each test. These tests fall into one or more of the following categories:

- shakedown and benchmark tests,
- nonpower pressure-drop tests,
- heat loss tests ("dry tests"),
- oxide-layer and water chemistry tests,
- nondestructive flow excursion tests,
- ANS nominal conditions,
- ANS off-nominal conditions,
- destructive flow excursion tests,
- critical heat flux tests, and
- wider span tests for scalability.

In the following section, the results of these tests will be discussed.

Table 1. THTL test and data summary

Test Case	Date	Q" av,c MW/m²	Q" ex,c MW/m²	V c m/s	dP ts,c MPa	P ex,c MPa	Tb in,c °C	Tb ex,c °C	$\Delta T_{sub,out,c}$ °C	Tw max,l °C	Heat Loss %,c	V 1 m/s	dP ts,1 MPa	Comments
Test Series: THTL-01; TSD-1/A; TS#: ST-01; Purpose: Preliminary benchmark; Termination: Quasi FE burnout @ edges; Comments: Extruded channel, dip-brazed flanges.														
HC122A	1/22/92	14.9	16.3	23.4		1.213	45.7	178.4	10.1		7.2			
Test Series: THTL-02; TSD-1/B; TS#: ST-03; Purpose: Preliminary benchmark; Termination: Edge burnout; Comments: Extruded channel, dip-brazed flanges.														
FE305A	3/5/92	3.0	3.2	7.1	0.098	0.506	45.8	133.5	16.9	182.81	7.8	14.91	0.393	
FE305B	3/5/92	6.1	6.6	14.4	0.352	0.513	46.4	133.3	19.6	188.56	4.1	24.97	1.017	
FE306A	3/6/92	5.8	6.3	9.0	0.164	1.708	44.7	178.8	25.8	237.66	8.1	20.02	0.658	
FE306B	3/6/92	11.9	13.6	19.9	0.663	1.692	45.6	169.6	34.5	248.73	6.2	26.12	1.076	
Test Series: THTL-03; TSD-1/C; TS#: ST-06; Purpose: Preliminary benchmark; Termination: Edge burnout; Comments: Extruded channel, dip-brazed flanges.														
FE408A	4/8/92	3.0	3.2	7.0	0.086	0.511	46.1	134.3	18.5	176.20	7.7	7.08	0.095	Variable heat flux
FE408B	4/8/92	5.5	5.9	14.4	0.307	0.510	50.0	128.2	24.5	172.76	9.9	14.53	0.346	Variable heat flux
FE416A	4/16/92	5.3	5.8	9.1	0.151	1.691	44.3	165.5	38.6	195.23	8.5	8.95	0.157	Variable heat flux
FE416B	4/16/92	8.2	9.1	14.1	0.338	1.720	44.7	164.6	40.3	237.33	6.8	14.11	0.360	Variable heat flux
FE424A	4/24/92	7.9	9.2	14.1	0.349	1.713	45.5	162.4	42.3	184.19	5.9	14.05	0.364	Variable heat flux
FE424B	4/24/92	11.4	13.2	19.5	0.690	1.689	45.6	166.8	37.2	253.62	5.3	19.45	0.656	Variable heat flux
FE428A	4/28/92	9.0	10.4	22.1	0.971	0.494	45.4	129.1	22.4	247.11	4.8	22.10	0.931	Variable heat flux
FE428B	4/28/92	9.0	10.2	19.2	0.856	0.499	45.5	142.4	9.5	245.57	5.4	28.00	1.493	
FE429A	4/29/92	8.8	9.7	13.3	0.438	1.707	45.3	183.7	20.8	263.98	7.3	23.99	1.083	
FE429B	4/29/92	11.8	14.2	18.8	0.723	1.710	45.5	176.2	28.4	352.94	6.7	27.98	1.499	
Test Series: THTL-04; TSD-3/A; TS#: 6782; Purpose: Add. benchmark; Termination: Premature edge burnout; Comments: Machined channel, welded flanges, thinner wall (36% H.F at edges).														
FE817A	8/17/92	No power.										26.60	1.254	
FE817B	8/17/92	No power.										26.60	1.254	
FE817C	8/17/92	6.2	6.7	8.1	0.119	1.653	44.0	182.5	20.2	233.57	6.8	17.20	0.456	Faulty edge weld (half penetration).
Test Series: THTL-05; TSD-3/B; TS#: 1292; Purpose: Add. FE benchmark, Termination: Gasket failed on exit flange. Depress. led to channel failure at exit.; Comments: Machined channel, welded flanges, thin wall (36% H.F.@ edges).														
FE903A	9/3/92	No power.										27.90	1.487	
FE903B	9/3/92	No power.										27.90	1.487	
FE904A	9/4/92	6.4	6.9	8.1	0.156	1.702	43.6	190.1	13.1	232.61	4.5	18.00	0.541	
FE904B	9/4/92	9.6	10.4	12.5	0.330	1.697	45.4	188.0	13.2	241.30	4.2	22.10	0.746	
FE904C	9/4/92	11.8	13.0	16.6	0.492	1.713	45.5	178.3	21.1	250.06	3.5	24.10	0.853	
FE904D	9/4/92	12.9	14.5	17.5	0.587	1.690	45.3	182.3	15.6	283.77	3.3	25.10	0.913	Teflon Gasket blew out. Rapid depress. led to failure.
Test Series: THTL-06; TSD-3/C; TS#: 141592; Purpose: Incr. H.F. FE tests; Termination: TS removed intact, opened for gap exam.; Comments: Mach. chan., welded flanges, thin wall, inlet & exit PTs moved to flanges.														
FEN17A	11/17/92	No power.										28.10	1.514	
FEN17B	11/17/92	9.3	9.9	12.5	0.296	1.721	45.2	182.5	22.7	205.43	7.6	22.20	0.764	
FEN17C	11/17/92	12.5	13.5	17.4	0.508	1.693	45.0	178.1	26.4	214.90	6.4	28.10	1.114	
FEN17D	11/17/92	No power.										28.10	1.491	
FEN19A	11/19/92	No power.										28.30	1.483	
FEN20A	11/20/92	13.7	15.1	19.0	0.604	1.725	45.5	178.6	26.9	232.91	6.3	30.00	1.269	
FEN20B	11/20/92	14.9	16.7	20.5	0.742	1.712	45.5	180.0	25.2	252.83	4.8	30.00	1.248	
FEN20C	11/20/92	No power.										28.00	1.468	
FEN30A	11/30/92	14.9	16.6	20.5	0.754	1.709	45.8	180.7	24.4	262.34	4.6	30.00	1.334	
FEN30B	11/30/92	No power.										30.00	1.643	
FED15A	12/15/92	No power.										40.20	2.771	
FED15B	12/15/92	12.7	13.7	17.1	0.545	1.706	44.4	181.9	23.0	238.15	5.5	28.00	1.147	
FED15C	12/15/92	13.8	14.9	18.6	0.632	1.719	44.0	181.3	24.1	252.39	5.1	36.00	1.877	
FED17A	12/17/92	14.6	16.3	20.5	0.747	1.685	44.4	178.8	27.7	275.45	6.1	36.00	1.906	
FED17B	12/17/92	No power.										36.10	2.244	
FED28A	12/28/92	No power.										30.00	1.619	
FED28B	12/28/92	14.8	15.5	20.0	0.765	1.723	44.2	181.1	24.4	241.99	5.5	35.90	2.070	
FE105A	1/5/93	No power.										38.00	2.878	
FE105B	1/5/93	9.4	10.0	13.5	0.359	1.721	44.4	173.6	31.6	237.07	6.2	26.10	1.278	
FE105C	1/5/93	12.7	13.8	17.5	0.657	1.722	44.1	179.1	26.3	263.49	4.9	30.10	1.670	
FE105D	1/5/93	14.9	15.9	20.0	0.919	1.707	44.3	182.5	22.6	265.47	4.4	36.00	2.539	
FE105E	1/5/93									71.60		34.10	2.509	Variable heat flux
FE105F	1/5/93	No power.										36.00	2.809	

Table 1. THTL test and data summary

Test Case	Date	Q" av,c MW/m²	Q" ex,c MW/m²	V c m/s	dP ts,c MPa	P ex,c MPa	Tb in,c °C	Tb ex,c °C	$\Delta T_{sub,ex,c}$ °C	Tw max,l °C	Heat Loss %,c	V 1 m/s	dP ts,1 MPa	Comments
Test Series: THTL-07; TSD-3/D; TS#: 1293; Purpose: Comp. FE to CHF (BPR=0.0); Termination: CHF Burnout near exit; Comments: Mach. chan., welded flanges, thin wall.														
FE114A	1/14/93	No power.										32.20	2.030	
FE114B	1/14/93	12.8	13.9	17.5	0.567	1.713	45.4	181.9	23.2	296.01	4.8	32.10	1.613	
CF115A	1/15/93	No power.										32.00	2.175	
CF115B	1/15/93	11.8	13.0	17.0	0.628	1.709	45.5	186.1	18.9	308.54	4.2	32.00	1.809	Minimum in demand curve
CF115B	1/15/93	12.8	13.7	12.2	1.262	1.860	48.0	208.7	0.2	308.44	5.0	32.00	1.809	Actual CHF Burnout
Test Series: THTL-08; TSD-3/E; TS#: 171892; Purpose: Actual FE (BPR=2.63); Termination: FE burnout); Comments: Mach. chan., welded flanges, thin wall.														
FE210A	2/10/93	No power.										36.00	2.807	
FE210B	2/10/93	12.6	14.6	17.5	0.618	1.718	45.6	178.2	27.1	272.97	5.9	32.10	1.838	
FE211A	2/11/93	No power.										36.10	2.809	
FE212A	2/12/93	12.6	13.7	16.7	0.653	1.708	45.7	185.2	19.7	464.75	5.6	32.10	1.891	Minimum in demand curve
FE212A	2/12/93	12.6	13.6	15.1	0.785	1.727	45.8	197.4	8.0	261.64	6.0	32.10	1.891	Actual FE burnout (BPR=2.63)
Test Series: THTL-09; TSD-3/F; TS#: 192093; Purpose: Actual FE @ Costa cond.'s (BPR=1.09); Termination: Unexp. early FE burnout; Comments: Mach. chan., welded flanges, thin wall.														
FE318A	3/18/93	No power.										16.00	0.696	
FE318B	3/18/93	2.2	2.5	4.5	0.078	0.445	37.6	132.7	15.1	172.86	12.4	15.00	0.522	Minimum in demand curve
FE318B	3/18/93	2.140	2.323	4.07	0.106	0.451	41.7	142.2	6.0	172.81	16.4	15.00	0.522	Actual FE burnout @ Costa cond.'s (BPR=1.09)
Test Series: THTL-10; TSD-3/G; TS#: 131693; Purpose: Bypass effect on actual FE @ 12 MW/m2 (BPR=6.15); Termination: Actual FE burnout.; Comments: Mach. chan., welded flanges, thin wall.														
FE329A	3/29/93	No power.										40.10	3.005	
FE330A	3/30/93	12.9	14.6	18.5	0.577	1.709	45.7	174.7	30.3	256.68	3.6	32.00	1.533	
FE330B	3/30/93	No power.										40.10	2.940	
FE331A	3/31/93	12.2	13.2	17.0	0.549	1.698	45.8	178.4	26.3	253.73	8.8	32.00	1.529	Minimum in demand curve
FE331A	3/31/93	12.1	13.1	15.8	0.634	1.696	45.8	187.3	17.2	253.23	9.6	32.00	1.529	Actual FE burnout @ (BPR=6.15)
Test Series: THTL-11 (2); TSD-3/H; TS#: 111293; Purpose: "Dry" & "Wet" tests for cond. heat losses; Termination: No failure but excess temp.'s; Comments: "Dark Oxide" buildup, Mach. chan., welded flanges, thin wall.														
HL420A	4/20/93			"Dry"								"Dry"	"Dry"	Initial leak on flange weld. Required buildup of weld material at inlet for first data series.
HL422A	4/22/93			"Dry"								"Dry"	"Dry"	Reversed test channel in backing, weld buildup now at exit, normal T/C config.
HL422B	4/22/93			"Dry"								"Dry"	"Dry"	Entire test section reversed, weld buildup at inlet, TT-101 now at inlet, etc.
HL428A	4/28/93			"Dry"								"Dry"	"Dry"	Config. same as HL420A, weld buildup at inlet, normal T/C config.
HL505A	5/5/93	12.9	16.5	27.1	1.066	1.727	45.5	135.7	70.35	293.36	3.7	27.24	1.174	Weld buildup at inlet, normal T/C config. test with flow. Trans. excess temp.'s near exit.
HL507A	5/7/93	No power.										33.36	1.945	Weld buildup at exit, TT-101 at inlet, test with flow. No power used.
HL507B	5/7/93	6.5	6.9	27.5	1.156	1.714	45.72	90.86	114.85	114.04	2.9	27.56	1.374	Weld buildup at exit, TT-101 at inlet, test with flow. Trans. excess temp.'s near inlet, had to stop power.
Test Series: THTL-12 (2); TSD-3/I; TS#: 4693; Purpose: Non-Boiling Base Case for Benchmark; Termination: "Black Oxide", Temp. increase in time; Comments: First test with ph control.														
BM611A	6/11/93	No power.	No flow.											
BM611B	6/11/93	6.3	7.2	13.8	0.382	1.687	45.9	127.6	76.62	201.03	4.8	38.14	2.595	
BM611C	6/11/93	6.4	7.4	16.0	0.503	1.696	45.9	118.4	86.17	189.00	2.1	15.99	0.503	Increasing velocity.
BM618A	6/18/93	No power.	No flow.											
BM622A	6/22/93	No power.	No flow.											
BM622B	6/22/93	6.2	7.2	13.9	0.392	1.701	46.0	126.8	77.80	221.70	5.3	35.66	2.276	
BM622C	6/22/93	6.4	7.4	17.8	0.659	1.683	45.9	110.4	93.9	207.60	3.1	17.85	0.687	
BM622D	6/22/93	No power.	No flow.									35.65	2.544	Black oxide and trans. temp. ramp., stop power. Oxide thick: 13 to 51mic. @ 400 to 490 mm fr. inlet
Test Series: THTL-13; TSD-3/J; TS#: 6793; Purpose: FE @ Pony motor & high flows cond.'s; Termination: Trans. temp. ramp leading to failure; Comments: Add. of nitric acid for ph contr.														
FE712A	7/12/93	No power.										26.78	1.441	
FE712B	7/12/93	1.9	2.1	2.5	0.033	1.695	42.7	183.1	21.1	214.39	12.2	16.05	0.526	
FE713A	7/13/93	No power.										10.22	0.318	
FE713B	7/13/93	0.8	0.8	2.7	0.025	0.175	43.3	100.1	16.2	124.66	15.1	10.96	0.306	
FE714A	7/14/93	No power.										0.00	0.016	

Table 1. THTL test and data summary

Test Case	Date	Q" av,c MW/m²	Q" ex,c MW/m²	V c m/s	dP ts,c MPa	P ex,c MPa	Tb in,c °C	Tb ex,c °C	$\Delta T_{sub,ex,c}$ °C	Tw max,l °C	Heat Loss %,c	V 1 m/s	dP ts,1 MPa	Comments
FE714B	7/14/93	5.3	5.8	7.5	0.142	1.700	44.2	174.3	30.2	225.59	6.5	21.99	0.896	
FE714C	7/14/93	7.4	8.1	10.0	0.248	1.701	45.9	182.3	22.2	228.37	5.5	26.09	1.186	
FE715A	7/15/93	No power.										20.22	0.891	
FE715B	7/15/93	10.3	11.9	14.5	0.440	1.709	45.9	177.0	27.9	289.29	3.1	32.07	1.651	
FE719A	7/19/93	No power.										31.03	1.824	
FE719B	7/19/93	12.5	15.4	17.5	0.634	1.673	45.9	176.8	27.1	374.31	3.8	34.06	1.768	Trans. temp. ramp with decreas. vel.
Test Series: THTL-14; TSD-3/K; TS#: 172094; Purpose: Flow Excursion and CHF type tests at previously tested conditions. Termination: Small crack at weld before CHF.														
FE322A	3/22/94	No Power										36.61	2.788	
FE323A	3/23/94	*6.3*	*6.5*	*36.6*	*2.444*	*1.712*	*44.5*	*76.4*	*128.2*	*88.79*	*6.1*	36.61	2.444	No Boiling, Data taken at the first data point.
FE323B	3/23/94	No Power										36.46	2.603	
FE324A	3/24/94	*12.6*	*13.3*	*36.5*	*2.210*	*1.776*	*44.9*	*108.7*	*97.0*	*156.95*	*6.0*	36.53	2.210	No Boiling, Data taken at the first data point.
FE324B	3/24/94	No Power										36.65	2.668	
FE324C	3/24/94	6.2	6.7	8.1	0.137	1.726	44.1	182.8	113.5	249.24	7.7	36.56	2.335	FE; Minimum in the demand curve.
FE324D	3/24/94	No Power												
CF328A	3/28/94	12.5	13.6	16.7	0.592	1.715	44.1	181.2	23.6	267.12	6.7	36.53	2.156	Minimum in the demand curve.
CF328A	3/28/94	12.6	13.2	11.7	1.098	1.847	44.1	208.4	18.4	264.41	6.2	36.53	2.156	Unexpected decreasing velocity transient causing CHF burnout.
Test Series: THTL-15; TSD-3/L; TS#: CD94; Purpose: Flow Excursion and CHF type tests at high heat flux conditions. Termination: Exit gasket failure leading to test section crack.														
FE506--	5/6/94													FE506 & FE509 aborted due to faulty flowmeter
FE509--	5/9/94													Data is considered suspect.
FE511A	5/11/94	No Power												
FE511B	5/11/94	16.9	17.9	21.5	1.074	1.700	44.5	185.8	18.2	259.84	5.2	35.96	2.313	
FE511C	5/11/94	19.0	20.1	24.5	1.432	1.680	44.4	184.1	19.6	273.76	5.2	36.02	2.522	
Test Series: THTL-16; TSD-4/A; TS#: 91094; Purpose: Flow Excursion and CHF type tests using a wide span test section (2.54 cm). Termination: CHF burnout.														
FE616A	6/16/94	No Power												
FE617A	6/17/94	No Minimum												Single Phase only @4MW/m²
FE620A	6/20/94	No Power												
FE620B	6/20/94	4.3	4.6	6.3	0.026	1.723	44.47	188.7	16.3	238.91	5.0	23.91	0.712	Minimum in demand curve
CF622A	6/22/94	6.5	7.1	9.7	0.103	1.726	44.37	185.9	19.2	248.44	4.2	24.01	0.68	Minimum in demand curve
CF622B	6/22/94	6.1	6.4	5.4	0.352	1.997	45.13	212.3	0.0	274.6	11.0	24.01	0.68	True CHF burnout
Test Series: THTL-17; TSD-3/M; TS#: 212994; Purpose: Measure time span for spallation front to strip oxide from channel wall. Termination: Transient burnout due to sudden loss of flow.														
FE715A	7/15/94	6.4	6.6	20.4	0.709	1.736	44.5	105.1	100.5	190.53	4.6	28.12	1.233	Test Section failed after a step change in velocity from 28 to 20 m/s. (Pump freq from 12 to 3.6 Hz)
Test Series: THTL-18; TSD-4/B; TS#: 6795; Purpose: Flow Excursion and CHF type tests using a wide span test section (2.54 cm). Termination: Structural failure unrelated to burnout.														
FE221A	2/21/95	No Power												
FE224A	2/24/95	5.5	6.0	8.7	0.161	1.699	44.1	185.3	19.8	252.6	12.8	25.06	1.01	further testing stopped after flange failure
FE613A	6/22/95	2.3	2.8	4.3	0.041	1.677	47.6	185.2	38.4	254.5	27.3	23.63	1.68	further testing stopped after unplanned test section failure unrelated to burnout phenomena

av - measured axial average
c - value at the minimum dP point
ex - exit (maximum)
Q" - heat flux
Tb ex - exit bulk coolant temperature
ts - test section
1 - value at the first data point of the case
l - value at point of lowest velocity

NOTES: (1)All tests were done with decreasing velocity at constant heat flux except as noted in comments.
(2)The THTL-11 and THTL-12 values are for the data with the lowest velocity (no minimum).

8. RESULTS OF THTL EXPERIMENTS

The results of the experiments will be presented and discussed in this section. The destructive and nondestructive FE experiments and a single CHF test will be discussed first, followed by the supporting experiments. Some anomalies and discrepancies in pressure drop, wall temperature, oxide buildup, and heat losses observed during some of the experiments were discussed in the FY 1993 Progress Report (Siman-Tov et al., 1994). Data analysis, correlation comparison, and conclusions will then follow.

8.1 NONDESTRUCTIVE FLOW EXCURSION TESTS

Most of the data taken in FY 1994 and 1995 were targeted for determining the thermal limits near or around the ANS nominal conditions, especially at very high heat fluxes and for the wider span test sections. The results of the FE tests performed so far are summarized in Table 2. Those performed during FY 1994 and 1995 are also represented in Fig. 14. The figures provide plots of the test section pressure drop vs velocity for constant heat fluxes as listed and for a single nonpowered case. Additional information on each run can be found in Tables 1 and 2. It was general practice to recheck a few of the pressure drop measurements as velocity was increased along the demand curve following the sequence where velocity was decreased to find the minimum. In some cases, the runs were duplicated for confirmation. The differences found in the velocities at the minimum pressure drop points were generally small, and the above-quoted velocities represent average values when multiple velocity measurements were made. However, in the high heat flux cases of 13 and 14 MW/m^2, pressure drops were higher when measurements were repeated for the same velocities. The heat fluxes indicated for each of these curves are nominal average values. The actual local heat fluxes close to the exit (where the FE phenomena is supposed to start) are indicated in Table 2 as the q''_{exit} values, which are higher than the average in all cases as a result of the aluminum resistivity change with temperature. As illustrated in Figs. 14 and 15, the minimum points are clearly identifiable, and a true CHF (or the subsequent expected burnout) was not encountered before that minimum (the point where FE would occur) in any of the experiments.

Acquiring FE data at this level of heat fluxes and velocities is of significance for two reasons. First, to the authors' knowledge, no data are available for velocities higher than 10 m/s (Duffey and Hughes 1990; Lee, Dorra, and Bankoff 1992; Rogers and Li 1992) except those reported by Waters (1966) at 16 m/s in experiments supporting the Advanced Test Reactor. Second, the heat fluxes achieved are beyond the ANS nominal peak heat flux of 12 MW/m^2 and almost as high as the ANSR local hot channel peaking factor of 18 MW/m^2. The corresponding limiting velocity tested is about 20 m/s, well below the ANS nominal velocity of 25 m/s. This implies, on a preliminary basis, that a good margin exists at the ANSR operating velocity. The THTL data taken so far is presented in Fig. 16 on a subcooling vs velocity plot mapped with various regimes of the ANSR possible operational requirements.

8.2 DESTRUCTIVE FLOW EXCURSION AND CHF TESTS

In addition to the above FE experiments, which are based on the minimum pressure drop (nondestructive tests), a number of destructive (actual burnout) tests were performed to compare true CHF using a "stiff" system to both destructive (actual burnout in a relatively "soft system") and nondestructive FE tests (minimum pressure drop in a "stiff" system). A total of three destructive FE and three true CHF experiments were performed so far, and the results are presented in Fig. 17.

Table 2. THTL critical data points for flow excursion and CHF tests.

TSD	Test Case	q''_{avg} (MW/m²)	q''_{exit} (MW/m²)	V_{exit} (m/s)	ΔP_{ts} (MPa)	P_{exit} (MPa)	$T_{bulk,exit}$ (°C)	$\Delta T_{sub,exit}$ °C	Heat Loss %
TSD-3/C	FEN17B	7.6	7.9	14.4	0.296	1.721	182.5	22.7	7.6
TSD-3/C	FEN17C	10.6	11.3	20.0	0.508	1.693	178.1	26.4	6.4
TSD-3/C	FEN20A	12.0	13.6	21.9	0.604	1.725	178.6	26.9	6.3
TSD-3/C	FEN20B	13.7	16.0	23.5	0.742	1.712	180.0	25.2	4.8
TSD-3/C	FEN30A	13.6	15.8	23.6	0.754	1.709	180.7	24.4	4.6
TSD-3/C	FED15B	11.6	13.0	19.7	0.545	1.706	181.9	23.0	5.5
TSD-3/C	FED15C	13.0	14.7	21.4	0.632	1.719	181.3	24.1	5.1
TSD-3/C	FED17A	14.4	16.1	23.5	0.747	1.685	176.8	27.7	6.1
TSD-3/C	FED28B	14.6	15.5	23.0	0.765	1.723	181.1	24.4	5.5
TSD-3/C	FE105B	9.0	9.9	15.4	0.359	1.721	173.6	31.6	6.2
TSD-3/C	FE105C	12.7	14.3	20.1	0.657	1.722	179.1	26.3	4.9
TSD-3/C	FE105D	14.8	16.3	23.1	0.919	1.707	182.5	22.6	4.4
TSD-3/D	FE114B	10.8	11.8	20.1	0.567	1.713	181.9	23.2	4.8
TSD-3/D	CF115B	11.8	13.0	19.8	0.628	1.709	186.1	18.9	4.2
TSD-3/D	CF115B*	11.8	13.0	14.5	1.262	2.840	209.2	21.6	4.5
TSD-3/E	FE210B	11.4	13.9	20.1	0.618	1.718	178.2	27.1	5.9
TSD-3/E	FE212A	12.1	13.3	19.3	0.653	1.708	185.2	19.7	5.6
TSD-3/E	FE212A*	12.1	13.0	17.8	0.785	1.738	194.8	10.6	7.4
TSD-3/F	FE318B	1.9	2.2	5.0	0.078	0.445	132.7	15.1	12.4
TSD-3/F	FE318B*	2.1	2.3	4.5	0.106	0.451	142.2	6.0	16.4
TSD-3/G	FE330A	12.0	14.0	21.1	0.577	1.709	174.7	30.3	3.6
TSD-3/G	FE331A	12.0	13.7	19.6	0.549	1.698	178.4	26.3	8.8
TSD-3/G	FE331A*	11.5	12.4	18.3	0.634	1.708	181.8	22.8	9.6
TSD-3/J	FE712B	1.7	1.9	2.9	0.033	1.695	183.1	21.1	12.2
TSD-3/J	FE713B	0.7	0.7	2.8	0.025	0.175	100.1	16.2	15.1
TSD-3/J	FE714B	4.3	5.0	8.6	0.142	1.700	174.3	30.2	6.5
TSD-3/J	FE714C	6.4	7.2	11.6	0.248	1.701	182.3	22.2	5.5
TSD-3/J	FE715B	9.2	10.8	16.6	0.440	1.709	177.0	27.9	3.1
TSD-3/J	FE719B	11.7	14.8	20.1	0.634	1.673	176.8	27.1	3.8
TSD-3/K	FE324C	5.6	6.5	9.4	0.137	1.726	182.8	22.0	7.7
TSD-3/K	CF328A	12.3	13.8	19.3	0.592	1.715	181.2	23.6	6.7
TSD-3/K	CF328A*	10.5	11.0	14.0	1.098	1.850	208.8	-0.3	6.2
TSD-3/L	FE511B	14.7	15.5	25.0	1.074	1.700	185.8	20.3	5.2
TSD-3/L	FE511C	16.8	17.9	28.4	1.432	1.680	184.3	21.6	5.2
TSD-4/A	FE620B	4.3	4.6	6.3	0.026	1.723	188.7	16.3	5.0
TSD-4/A	CF622B	6.5	7.1	9.7	0.103	1.726	185.9	19.2	4.2
TSD-4/A	CF622B*	6.1	6.4	5.4	0.352	1.997	212.3	0.0	11.0
TSD-4/B	FE224A	5.5	6.0	8.7	0.161	1.699	185.3	19.8	12.8
TSD-4/B	FE613A	2.3	2.8	4.3	0.041	1.677	165.2	38.4	27.3

I. In all cases the inlet temperature is nominally 45 °C, except for FE318B where the inlet temperature is 40°C.

II. The critical point refers to the minimum pressure drop data point for most Flow Excursion tests. The asterisk (*) symbol refers to a true destructive burnout.

III. TSD-3 has a span of 12.7 mm; TSD-4 has a span of 25.4 mm.

IV. Nomenclature:

(All values refer to the critical data point)

- q''_{avg} average nominal heat flux
- q''_{exit} local exit heat flux
- V_{exit} exit coolant velocity
- ΔP_{ts} test section pressure drop
- P_{exit} exit pressure
- $T_{bulk,exit}$ exit bulk coolant temperature.
- $\Delta T_{sub,exit}$ exit subcooling

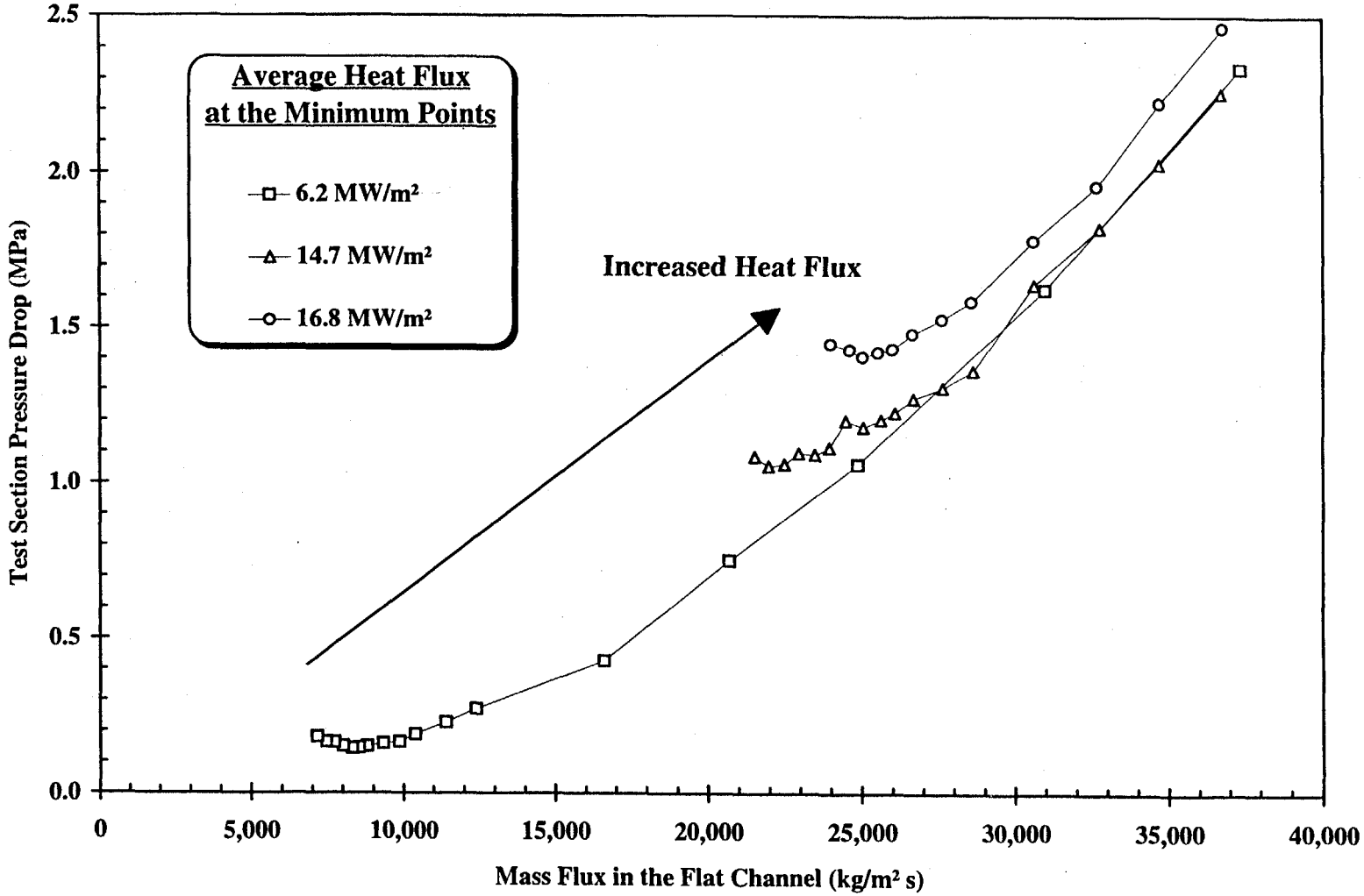

Fig. 14. FY 94-95 flow excursion data from THTL experiments with nominal span (12.7).

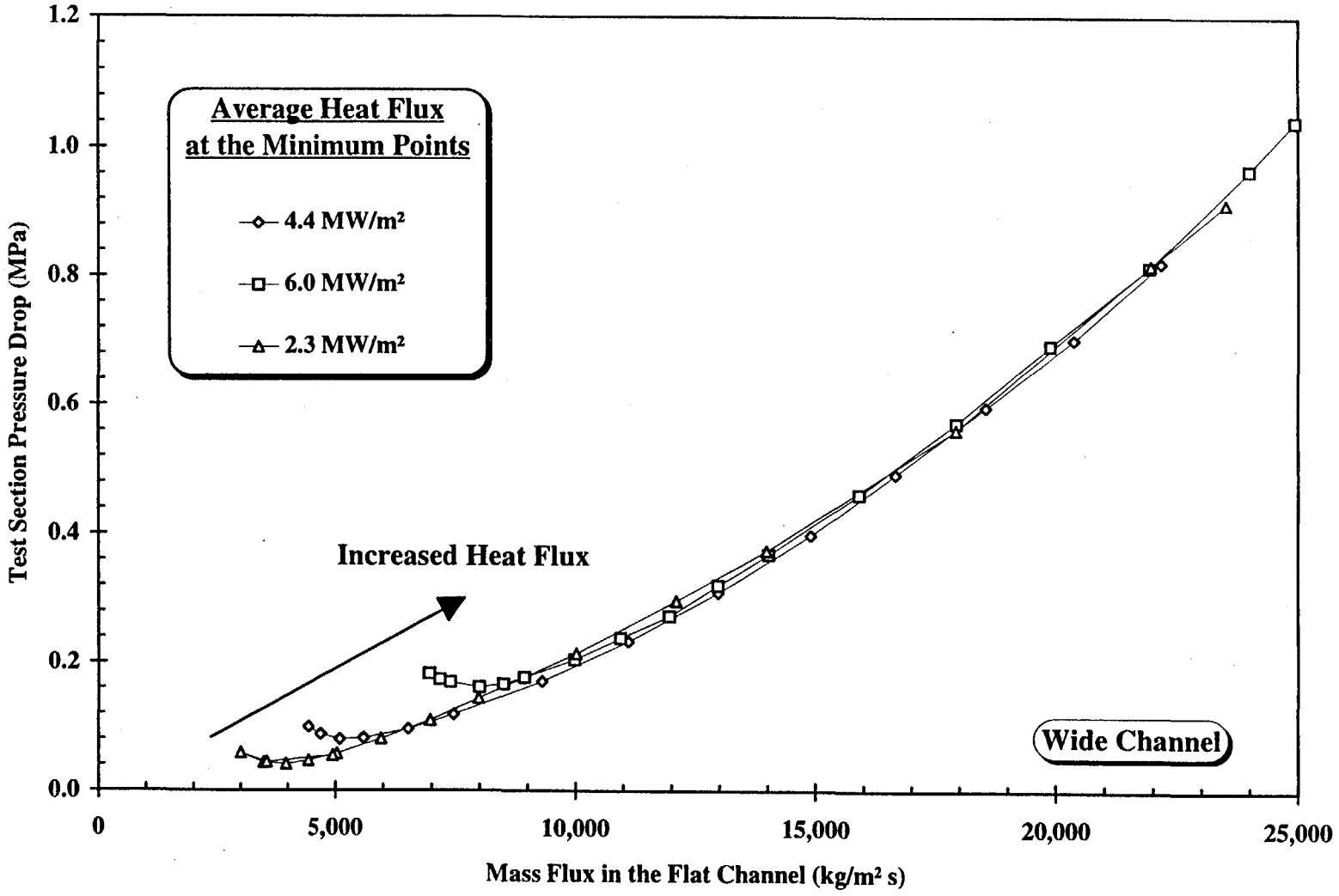

Fig. 15. FY 94-95 flow excursion data from THTL experiments with wide span (25.4).

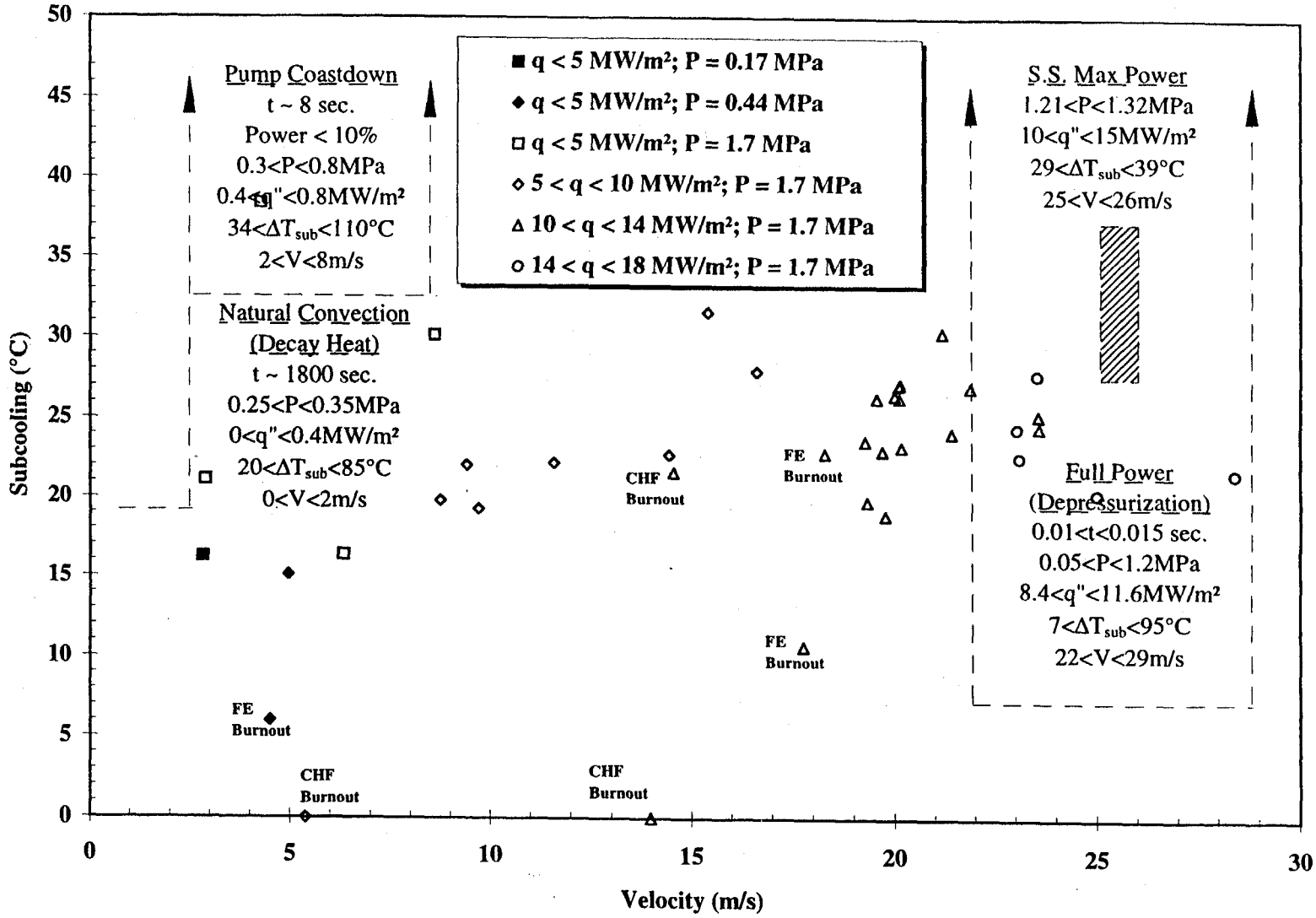

Fig. 16. THTL flow excursion data in relation to ANSR regimes.

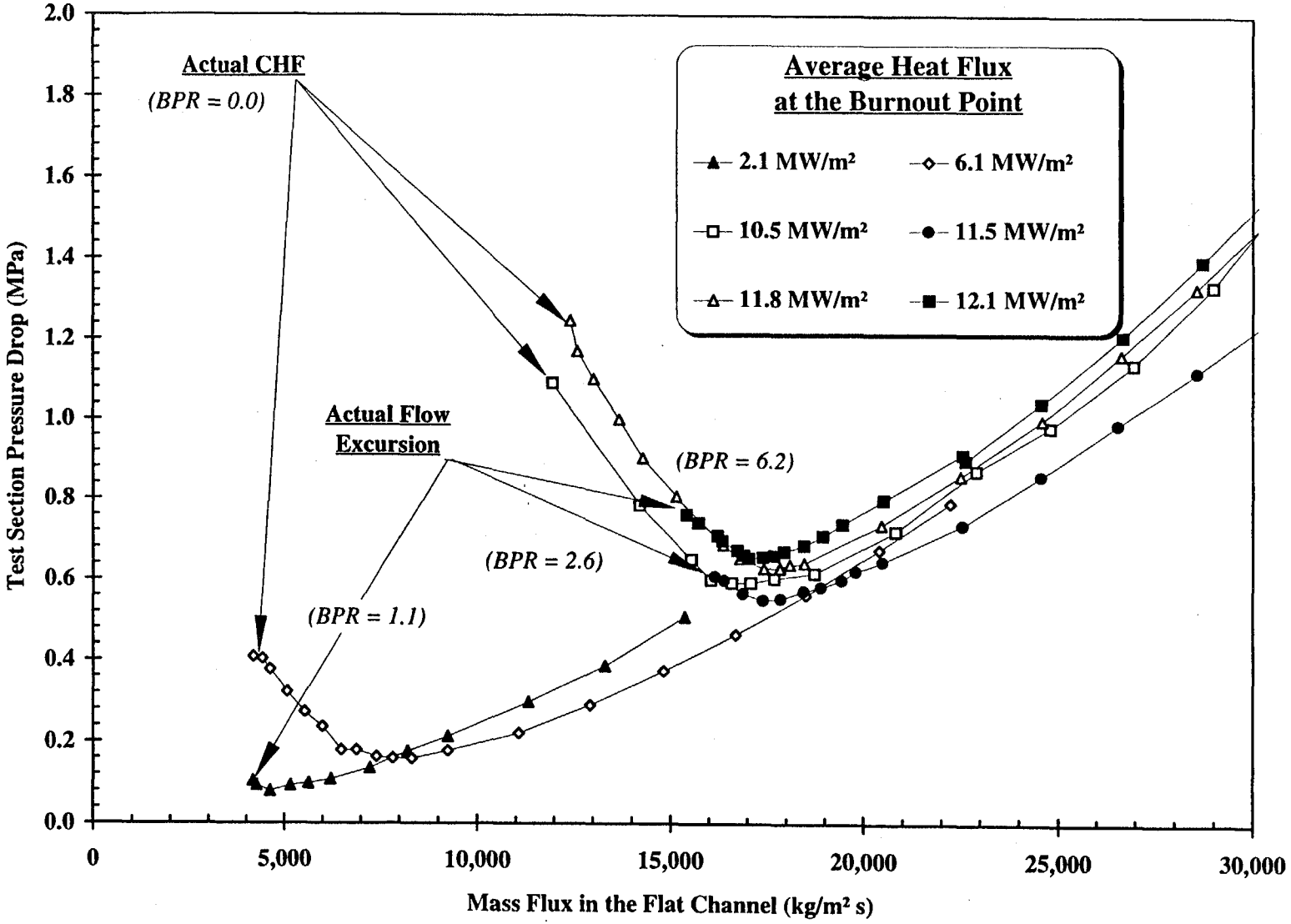

Fig. 17. Destructive CHF and FE tests performed in the THTL.

8.2.1 Burnout CHF Tests

The three CHF experiments were performed in a "stiff" system with a closed bypass line. The occurrence of CHF was clearly identified in the experiments by a rapid burnout and failure of the test channel. The CHF shows an average of about 30% additional margin in velocity for the two regular span tests and about 40% for the single wide-span test compared to the FE values at the minimum pressure drop, which are clearly identifiable in Fig. 17. This large margin between CHF and FE was somewhat surprising. The CHF results for the regular span tests agree quite well with data by Boyd (1989) taken under similar conditions but with subcooling of 65°C (compared to no subcooling in our experiment). Comparison of these THTL experimental results with either Boyd's test or ANSR nominal conditions also is not quite proper because the exit subcooling levels are much lower for the THTL experimental case. To achieve CHF with all the conditions similar to those of Boyd or nominal ANSR (including exit subcooling), a much shorter test section length is necessary. However, under such conditions, the expected CHF would be even higher.

It should be noted that these results are preliminary and a number of factors must be taken into account in evaluating the data. The local heat flux at the exit end of the test section is normally higher than the channel average heat flux because the coefficient of electrical resistivity for aluminum varies with temperature. Under such conditions, it is expected that the CHF burnout will occur at or very near the end of the heated channel. Inspection of the channel after opening showed, however, that the CHF burnout occurred about 2.5 cm upstream of the channel exit (the channel was missing from ~1.5 cm to 3.5 cm from the outlet end). This could be due to conduction cooling effects of the relatively massive electrode flanges that form the boundary for the "heated" length (see Sect. 6.2). This cooling effect reduces the heat flux actually transferred to the coolant near the exit, and the internal wall temperatures are artificially lowered, sometimes to levels below the temperatures observed upstream. In addition, the spanwise heat losses suggested by the oxide layer-profile observed on the test channel wall probably need to be accounted for.

The main conclusion from these tests is a confirmation of the assumption (also demonstrated by other researchers under different T/H conditions) that the minimum pressure drop technique for determining FE conditions is a conservative way to determine the FE point since it implies a complete constant pressure boundary condition as will be the case for an "infinite bypass." Increasing the bypass ratio from 2.6 to 6.1 gave a closer agreement with the minimum point, but higher ratios will apparently be needed to get a closer match. This, however, is not necessary if we accept the conservatism involved in the minimum pressure drop approach.

8.2.2 Burnout Flow Excursion Tests

Three destructive FE experiments were performed in a "soft" system, but each with a different bypass ratio (BPR), as indicated in Fig. 17. The tests were designed to compare the nondestructive FE test (based on minimum pressure drop criteria) with an actual destructive FE in order to validate our belief that the minimum in the pressure drop vs flow rate curve of a single channel represents a true FE condition for multiple channels. Three BPRs of 1.1, 2.6, and 6.2 and the results were discussed in Siman-Tov et al. (1994).

8.3 SUPPORTING TESTS AND OBSERVATIONS

A number of tests were performed primarily to investigate some assumptions and unusual observations. Those discussed in the 1993 Progress Report (Siman-Tov et al., 1994) included pressure and temperature measurements, oxide layer build-up, axial and spanwise heat redistributions, and heat losses to flanges and the massive electrodes. One major concern involved some inconsistent T/C measurements evidenced by both large differences between "redundant" T/Cs (east and west) and by inconsistencies in measurements along the channel. Therefore, some experiments during 1994–1995 were performed and sequenced to help investigate these inconsistencies. These included some experiments with ΔP vs V data at no power, followed by sequences with power but no boiling (FE323A at 6 MW/m^2 and FE324A at 12 MW/m^2), and finally with power, boiling,

and the standard flow excursion minimums (FE324C at 6 MW/m^2 and CF328A at 12 MW/m^2). One reason for performing these tests in such a sequence was to investigate the causes for inconsistencies in the T/C measurements that we have observed in the past, evidenced by large differences between "redundant" T/Cs (east and west) and along the channel. These differences seem to increase with temperature and were as high as 25–30°C, although most were below 10°C. Analysis of the T/C data indicates that the main problem might be inconsistency in the T/C's contact resistances.

Figure 18 shows, for the no-boiling test FE324A (12 MW/m^2), the temperature difference between east and west plotted against the average temperature at each T/C elevation (marked by section number). As can be seen, in almost all cases, this difference increases with the average temperature, indicating a possible effect of contact resistance variations. Sections 1, 7, 8, and 9 have different T/C types on east and west, and, indeed, the average temperature for those locations are the highest. However, this does not seem to be the only contributor to those discrepancies. Figures 19-22 show the temperatures measured, the temperatures that could be expected in the corresponding T/C locations based on Petukhov heat transfer coefficient (if no oxide layer is present and no span-wise heat redistribution is assumed), and the temperature difference between east and west, for four data points from four different successive tests. There was no boiling for any of the four data points. The first and the third have the same T/H conditions and so do the second and the fourth. The following conclusions can be derived from these plots:

1. The differences between east and west are consistent in all four cases and also with what was presented in Fig. 18. That probably implies that those differences are primarily a result of differences in T/C contact resistance (especially locations 1, 7, 8, and 9 which have different T/C types in east and west). Improvement in T/C contact resistance could possibly be achieved by changes in spring tension and/or use of T/C contact cement.
2. The measured temperatures increase with time (sequence of tests) for the same T/H conditions (compare the first test to the third at 6 MW/m^2 and the second test to the fourth at 12 MW/m^2), especially toward the channel exit. This probably implies that the oxide layer builds up continuously with time and that the growth rate is higher toward the exit where the temperatures and heat fluxes are higher.
3. The first test (FE323A05) did not have much time for any oxide buildup and the temperature differences between east and west T/Cs are small in comparison to the overall differences between predicted and measured. This implies that the heat flux at the T/Cs midplane is lower than calculated from the electric field, even after reducing the overall heat losses to the outside (about 6.7% in this case). This additional "heat loss" may be in the form of heat redistribution from the T/Cs midplane in the span-wise direction that is dumped into the colder fluid at the corners of the channel. Assessment of this heat redistribution indicates an approximate level of about 12% heat redistribution in addition to the 6.7% of heat loss to the outside of the test section.
4. Approximate post-test measurements of the oxide layer thickness at different elevations for different test sections indicates a general trend of oxide buildup with time and temperature. The thickness measurements (admittedly not very accurate) range as high as 22 microns. These measurements confirm the general conclusions expressed above. The oxide layer thicknesses involved can easily explain much of the gap between expected and measured temperatures (depending on how much heat redistribution is assumed).

The above analysis indicates that we have four sources of errors: (1) heat losses to the outside of the test section, which is not uniform and is much larger toward the channel exit (the total, however, can be calculated with relative confidence); (2) heat redistribution in the span-wise direction from the T/Cs midplane to the colder fluid in the channel corners; (3) a relatively fast oxide layer growth rate that is especially high toward the channel exit (the probable cause for this accelerated oxide buildup is the pH level, which is currently not controlled and is at higher levels than the pH of 5 used in the corrosion test loop and nominally specified for the ANSR); (4) inconsistencies in T/C measurements resulting probably from imperfect T/C contact resistance. Even though all four factors seem to be important, the dominating uncertainties are in heat redistribution and oxide buildup.

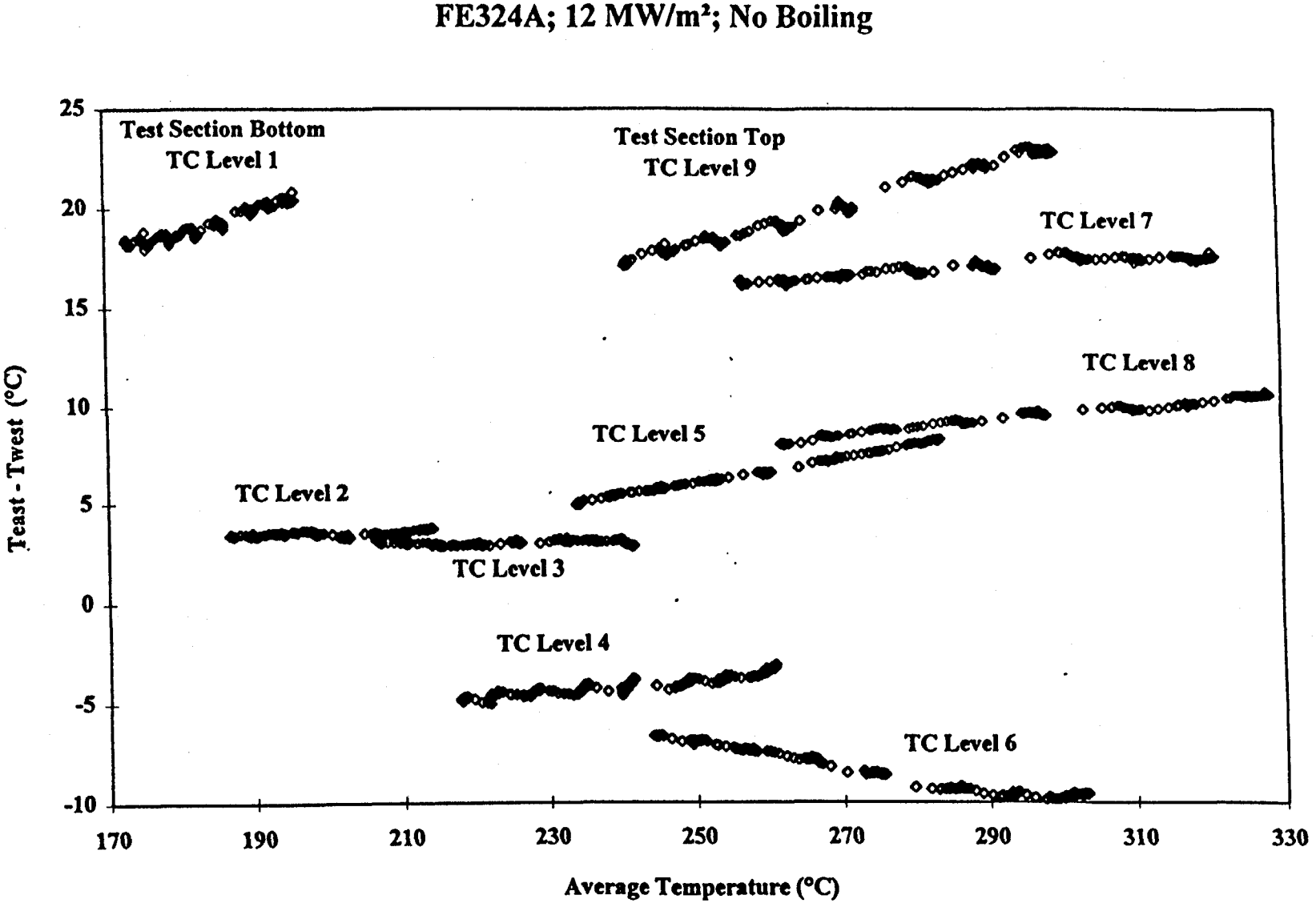

Fig. 18. Measured temperature differences between east and west sides at various thermocouple elevations.

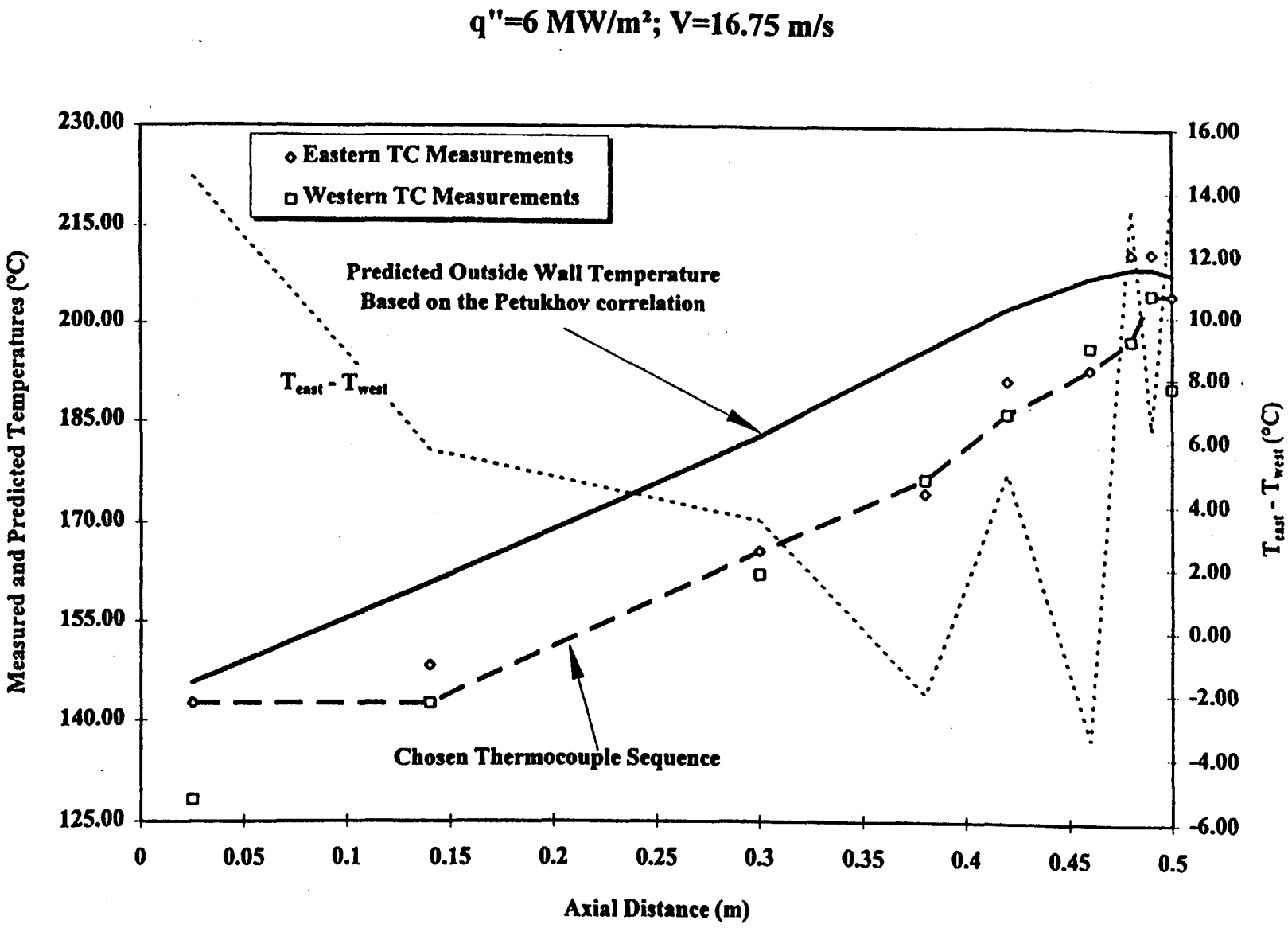

Fig. 19. Measured and expected temperatures at no-boiling conditions for test point FE323A05.

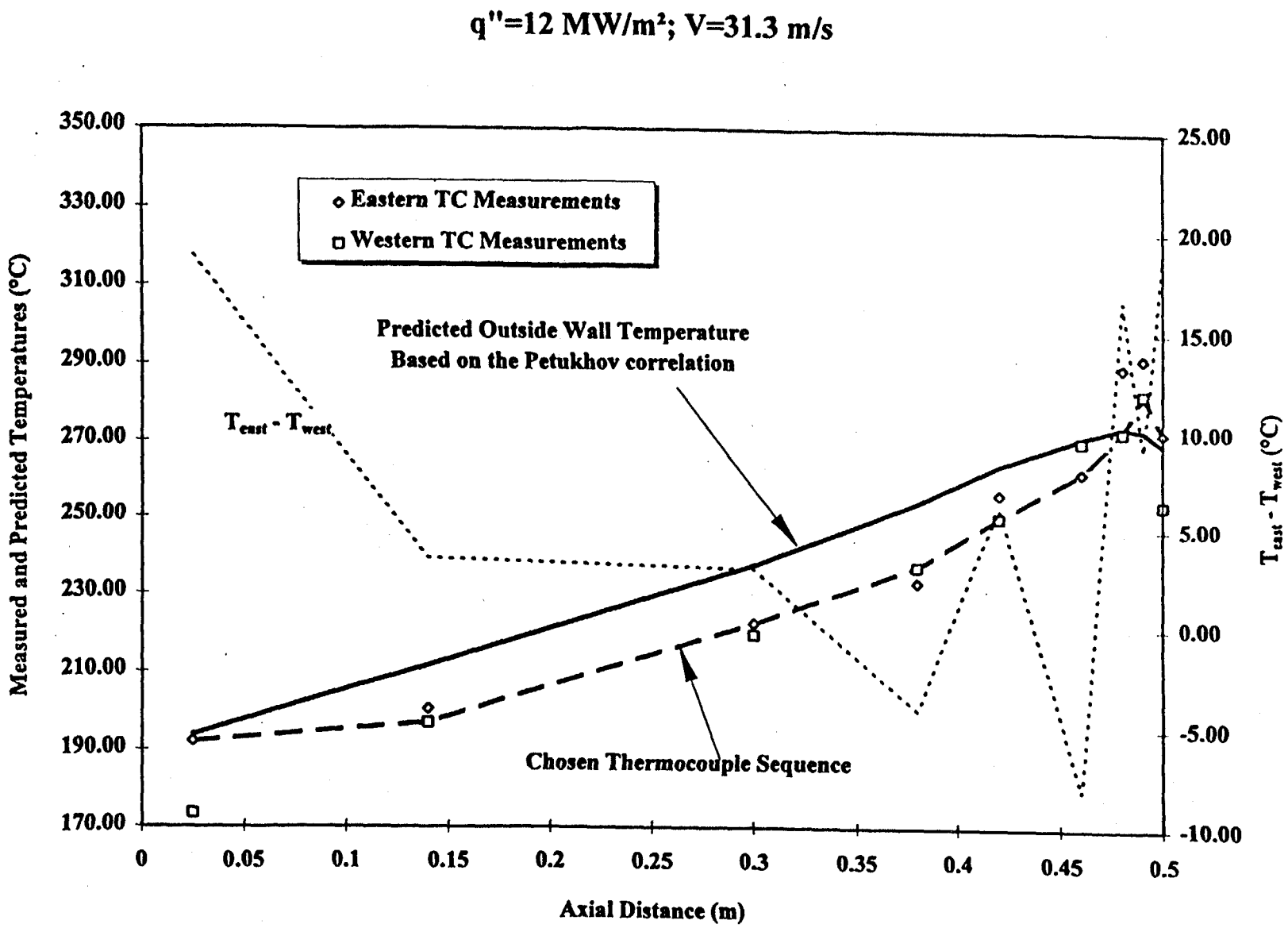

Fig. 20. Measured and expected temperatures at no-boiling conditions for test point FE324A04.

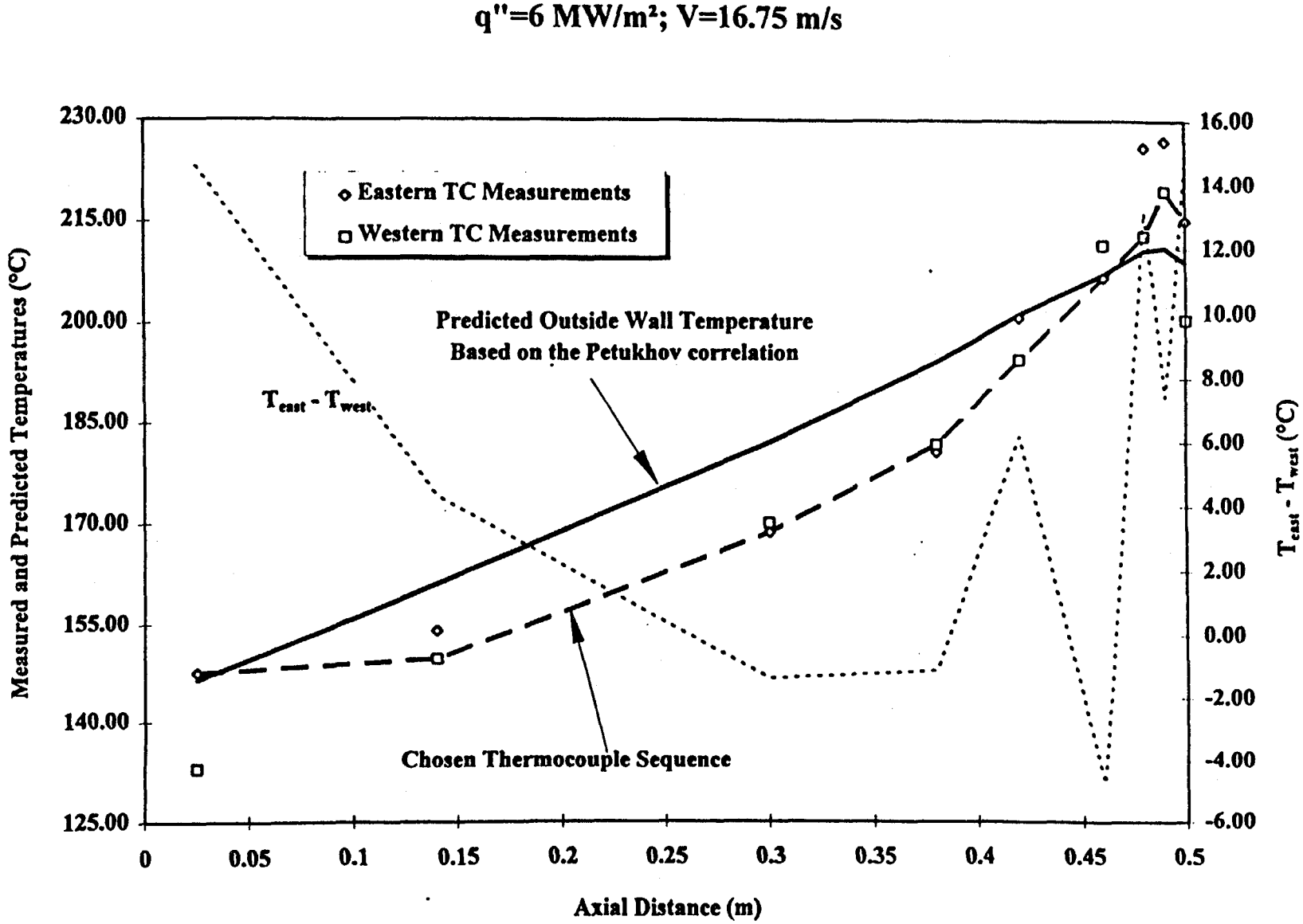

Fig. 21. Measured and expected temperatures at no-boiling conditions for test point FE324C05.

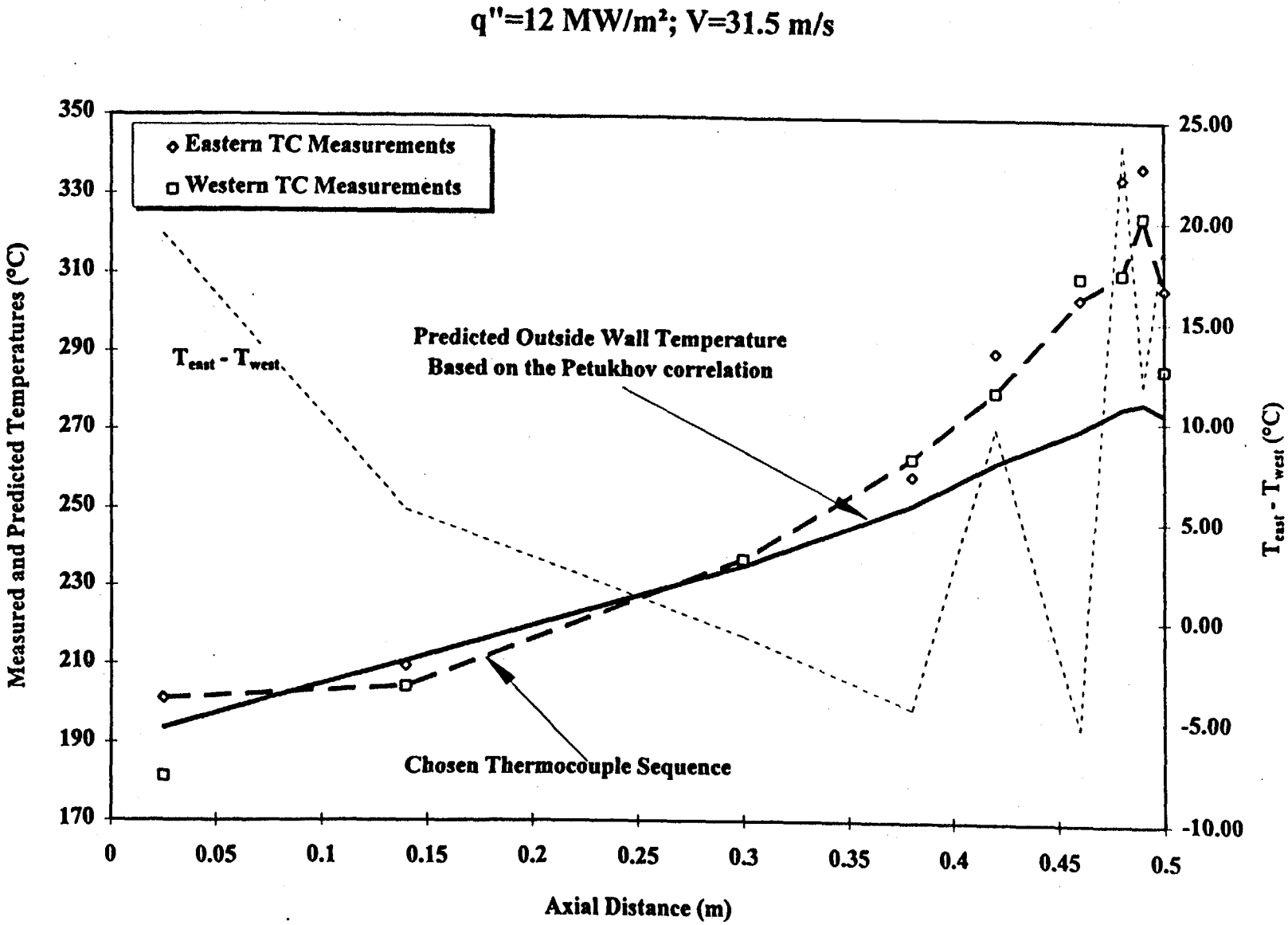

Fig. 22. Measured and expected temperatures at no-boiling conditions for test point CF328A04.

Another type of unusual behavior occurred during the test CF328A. The intent in this test was to continue to CHF after achieving the FE minimum. However, as indicated earlier, the approach to the test section failure was not as normally would be expected for a CHF test. With no change in pump speed and the bypass being completely closed, a velocity decrease started at ~13 m/s and intensified gradually down to ~11.5 m/s when the test channel failed (evident by steam release but no dramatic sound or light). Post-test inspection of the test channel and the transient data close to the failure time were used to develop a scenario of the event. The flow started to decelerate as the resistance to flow in the test section increased with additional vapor generation. Since the pump speed was maintained constant and the bypass was closed, the flow decrease probably occurred because of some "softness" in the pump itself (the pump characteristic not quite having a constant flow with pressure-drop). At a velocity of ~11.5 m/s, a crack occurred in the test section that compromised its pressure boundary to atmospheric pressure, causing both inlet and exit pressures to decrease in a way that the net pressure-drop also decreased. Being in the two-phase mode, the flow accelerated up to the "minimum" point of the test section demand curve and then decelerated as the system pressure continued to fall (Fig. 23). The power cutoff was triggered by low pump suction pressure caused by the decreasing test section exit pressure. The maximum temperature recorded was only 374°C, well below the melting point. However, because of the time response of the Tcs, this does not exclude a very brief and local temperature spike, which can explain the limited melting observed in a single small spot on the back of the test section. The conclusion so far, however, is that we had a partial slow "flow excursion" (decrease in velocity) leading to a thermal stress (crack) failure of the test section at a point very close to CHF (but not a typical CHF, which normally involves an extreme temperature excursion and melting, especially if the material is aluminum).

8.4 EVALUATION OF EXPERIMENTAL UNCERTAINTIES

The uncertainties in the THTL experiments are discussed and evaluated in Sect. 6 as part of the data reduction process. As can be seen in Table 3, the standard deviation in the final calculated parameters, the *St* number and the *Nu* number, are in the 6–6.5% range. This is relatively low level for such a complicated set of experiments.

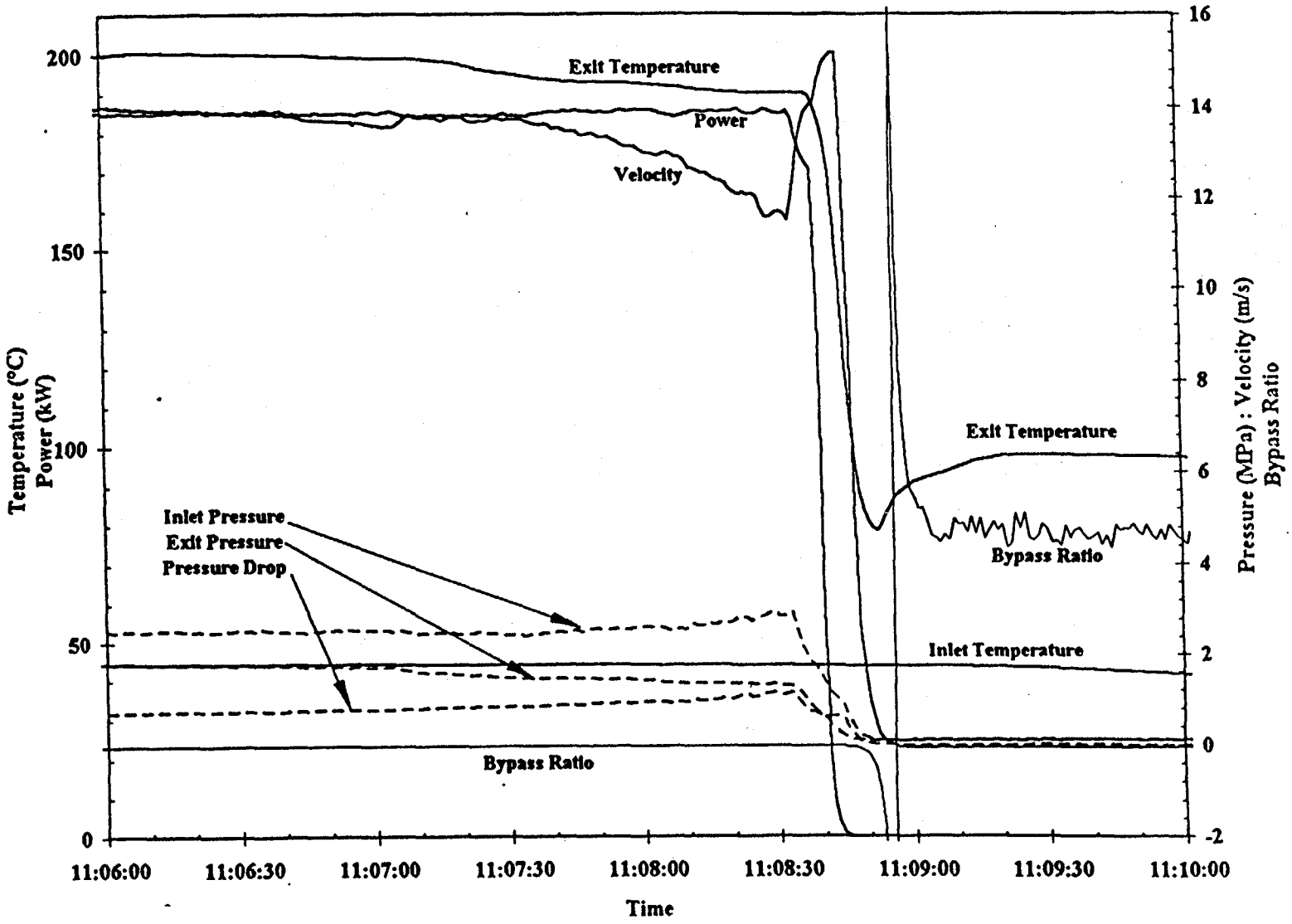

Fig. 23. Transient behavior in THTL-14 and CHF tests (CF328A) close to failure.

Table 3. U factor[a] statistics for Costa, S&Z, and Modified S&Z correlations[c]

Peclet range	Correlation	Data range	# Points	Average	S.D.[b]	S.D. %
Pe > 70,000 (Stanton Correlation)	Costa	THTL data	28	1.50	0.35	23.4
		All data	633	1.18	0.76	64.6
		V > 8 m/s	104	1.87	0.78	41.9
		V < 8 m/s	529	1.04	0.68	65.2
	Saha & Zuber	THTL data	28	1.07	0.24	22.4
		All data	633	1.40	0.73	51.7
		V > 8 m/s	104	1.40	0.62	44.3
		V < 8 m/s	529	1.40	0.75	53.1
	Modified Saha & Zuber	THTL data	28	1.03	0.16	15.9
		All data	633	1.02	0.30	29.7
		V > 8 m/s	104	1.10	0.20	18.6
		V< 8 m/s	529	1.00	0.31	31.5
Pe < 70,000 (Nusselt Correlation)	Saha & Zuber	THTL data	3	0.75	0.41	54.9
		All data	168	1.28	0.85	66.4
	Modified Saha & Zuber	THTL data	3	0.62	0.31	50.9
		All data	168	0.84	0.55	66.0

[a]U = Experimental heat flux/predicted heat flux.

[b]S.D. = Standard deviation of U.

[c]Excludes a data point with very low exit subcooling of 0.14°C (see Fig. 4). This data, if included, will increase considerably the S. D.s for the Costa and S&Z correlations and somewhat improve them for the proposed modified correlation.

9. DATA COMPARISON AND CORRELATION

The THTL data was compared with a number of correlations in order to select the most appropriate one for the ANSR application. The selected correlation was further evaluated by comparison to the much larger ANS data base for FE and OSV from the open literature. As a result, a modified Saha & Zuber correlation was proposed for the ANSR application. This process will be briefly covered in the following sections. A more detailed description of this material is given by Siman-Tov et al., (1991, March 1995, April 1995, and 1996.)

9.1 COMPARISON OF DATA TO CORRELATIONS

The collected data so far, including the FE tests under normal conditions (THTL-13), were plotted for comparison to selected correlations in Fig. 24. The uncertainty bars for each test reflect uncertainties connected with nonuniform axial heat losses and internal spanwise heat redistribution in the test section, as discussed previously in relation to multidimensional effects. The comparisons are made with correlations by Costa (1967), Whittle and Forgan (1967), and Saha and Zuba (1974). The Costa correlation is the one currently being used for the preliminary ANSR T/H design and analysis. Whittle and Forgan (W&F) and Saha and Zuber (S&Z) correlations are widely used in the United States, with the S&Z correlation being well established in many computer codes for nuclear safety analysis. For a given coolant (water), physical properties, and geometry (L/D = 199.6), all three correlations can be rearranged and simplified to the same general formulation, as follows:

$$\frac{q_{fe}}{(T_s - T_b)_{fe}} = C V^n \quad . \tag{22}$$

where C = 1/0.0128 and n = 0.5 (Costa); C = 1/0.0382 and n = 1.0 (S&Z); and C = 1/0.0427 and n = 1.0 (W&F).

In the Costa correlation, the FE heat flux is proportional to the square root of velocity, whereas both W&F and S&Z (as well as most other FE correlations) show a linear dependence. Based on this formulation, the Costa correlation will yield the same result as the W&F correlation at a velocity of 11.1 m/s and, in comparison, will be too optimistic (higher heat flux) at lower velocities and too conservative at higher velocities (33% more conservative with respect to W&F at the ANSR nominal velocity of 25 m/s). The Costa correlation will show the same trend when compared with the S&Z correlation, except that the equality will occur at 8.9 m/s. At 25 m/s, the Costa correlation will be ~40% more conservative with respect to the S&Z correlation.

Since the above correlations are based on data for relatively low velocities (maximums of 9.14, 7, and 7.66 m/s for W&F, Costa, and S&Z, respectively), it is quite interesting to see the trend of our data in terms of dependence on velocity. As can be seen in Fig. 24, all three correlations seem to be generally conservative when compared with the data, with S&Z being the most accurate. Excluding three of the four data points taken with test section TSD-3/B (a possible anomaly with this test section is being investigated), the agreement with S&Z is quite good, with the correlation skirting the lower bound of the data. The nominal conditions data points (indicated in the figure by TSD-3/J) are in good agreement with S&Z and W&F correlations but show again the Costa correlation to be too conservative in the high-velocity range but (unexpectedly) somewhat optimistic at the lower-velocity range. The FE heat flux dependence on velocity seems to be between 0.5 power (Costa) and 1.0 (S&Z and W&F), more nearly in the 0.8–0.9 range. This heat flux estimation is in agreement with the conclusion recently arrived at by Lee and Bankoff (1992) and Rogers and Li (1992), who relate the heat flux to the turbulent heat transfer coefficient, which is approximately proportional to the 0.6–0.8 power of velocity. As indicated before, the actual correlation of the ANSR FE data will be postponed to a later stage.

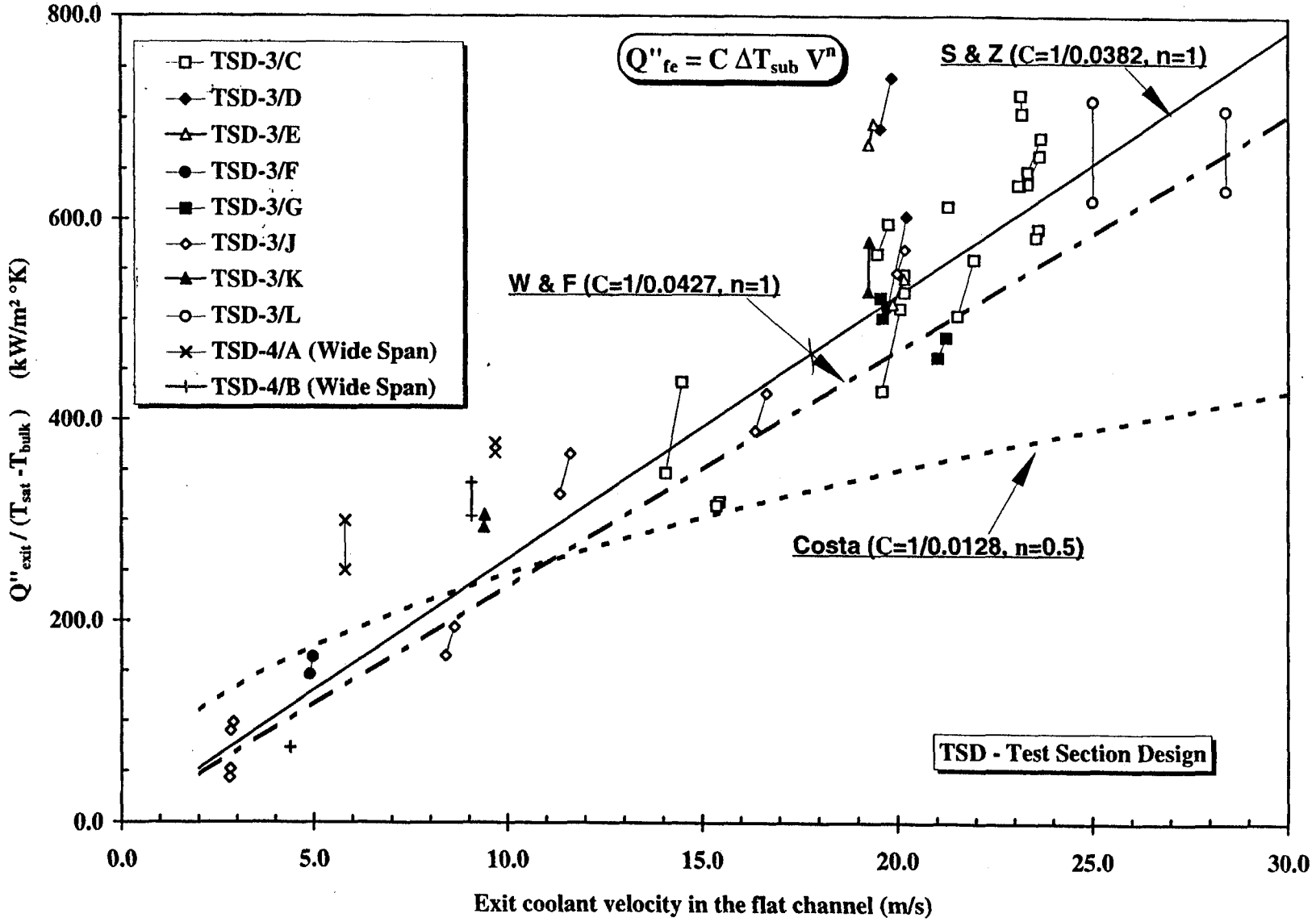

Fig. 24. Comparison of THTL FE data with correlations.

An interesting comparison of the FE data and the single CHF data point with the Gambill/Weatherhead CHF correlation is presented in Fig. 25. As can be seen, the FE data show quite a good agreement with the Gambill/Weatherhead CHF correlation, whereas the correlation is about 50% conservative in relation to the single CHF data point taken so far. This could indicate that the Gambill/Weatherhead correlation is more closely representing FE phenomena than CHF (depending on how "soft" the actual experimental system may have been). More CHF data are required (as is indeed planned) to come to any reliable general conclusion on the CHF correlation performance.

The above data comparison supported a shift from the Costa correlation to the S&Z correlation for the ANSR, especially since the nominal conditions of most of the accident scenarios analyzed in the ANSR involve rather high mass fluxes. Although it is a reasonable selection based on direct data comparison, the W&F correlation was not selected because of its global rather than local nature. This characteristic of the W&F correlation becomes a major liability for nonuniform heat flux distributions, which exist both axially and span-wise in the ANSR and when statistical uncertainties are applied in the analysis.

The S&Z correlation seems to be a good selection for the ANSR conditions because it represents the data quite well over the entire range of interest. However, the limiting heat flux based on the original S&Z correlation is very sensitive to the subcooling value at low subcooling and decreases to zero as subcooling reaches zero. This is obviously unrealistic since the FE heat flux cannot be lower than the IB heat flux. Therefore, it became useful to plot the THTL data in terms of the *St* and *Nu* numbers (which are the selected dimensionless groups in the original S&Z correlation) against subcooling as shown in Fig. 26.

As can be seen in the figures, there is a clear trend for the *St* number to increase with declining subcooling, particularly at lower subcoolings. In addition, it should be observed that by definition both the *St* and *Nu* numbers must become infinite when the subcooling is zero, which contradicts the constant values for these parameters suggested by the original S&Z correlation. On the other hand, as can be seen from Fig. 27, the data does not show any meaningful trend of *St* with respect to velocity. These observations provide a strong case for modifying the S&Z constant *St* number (0.0065) and constant *Nu* number (455) criteria, in relation to subcooling, especially in the low subcooling range.

9.2 PROPOSED APPROACH TO CORRELATIONS

A limited investigation led to recommended preliminary modifications to the S&Z correlation. A best fit was developed based on the 505 data points of the ANS data base for FE presented by Siman-Tov et al. (1995), including 26 data points from THTL. Under guidelines and constraints listed in Siman-Tov et al. (1995), the following subcooling correction factor was employed to improve the original S&Z correlations for the ANS applications:

$$St = q''/(G \; C_p \; \Delta T_{sub}) = 0.0065 \; \eta_{sub} \quad , \qquad Pe < 70{,}000 \quad ; \tag{23}$$

$$Nu = q'' \; D_h \; /(k\Delta T_{sub}) = 455 \; \eta_{sub} \quad , \qquad Pe < 70{,}000 \quad ; \tag{24}$$

where $\eta_{sub} = 0.55 + 11.21/\Delta T_{sub}$ (η_{sub} being the proposed subcooling correction factor).

Figures 28 and 29 show the selected modified correlations in terms of *St* number and *Nu* number, respectively, against the expanded ANS data base (802 data points, including 31 from THTL tests). Table 3 provides the statistics for the modified S&Z correlation in terms of mean and standard deviation, as well as for the original S&Z and Costa correlations for the same data base.

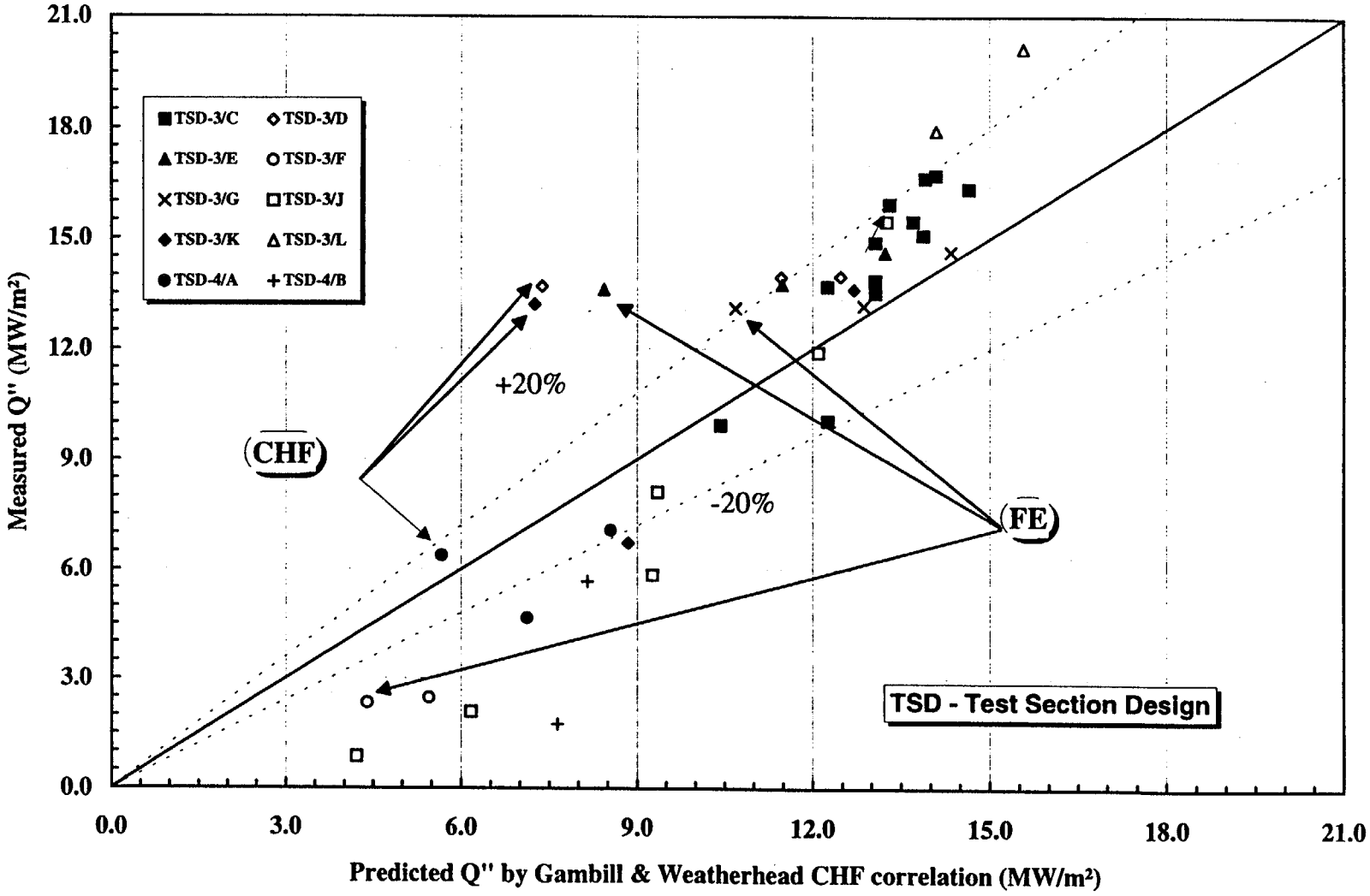

Fig. 25. Comparison of THTL FE data with the Gambill/Weatherhead correlation.

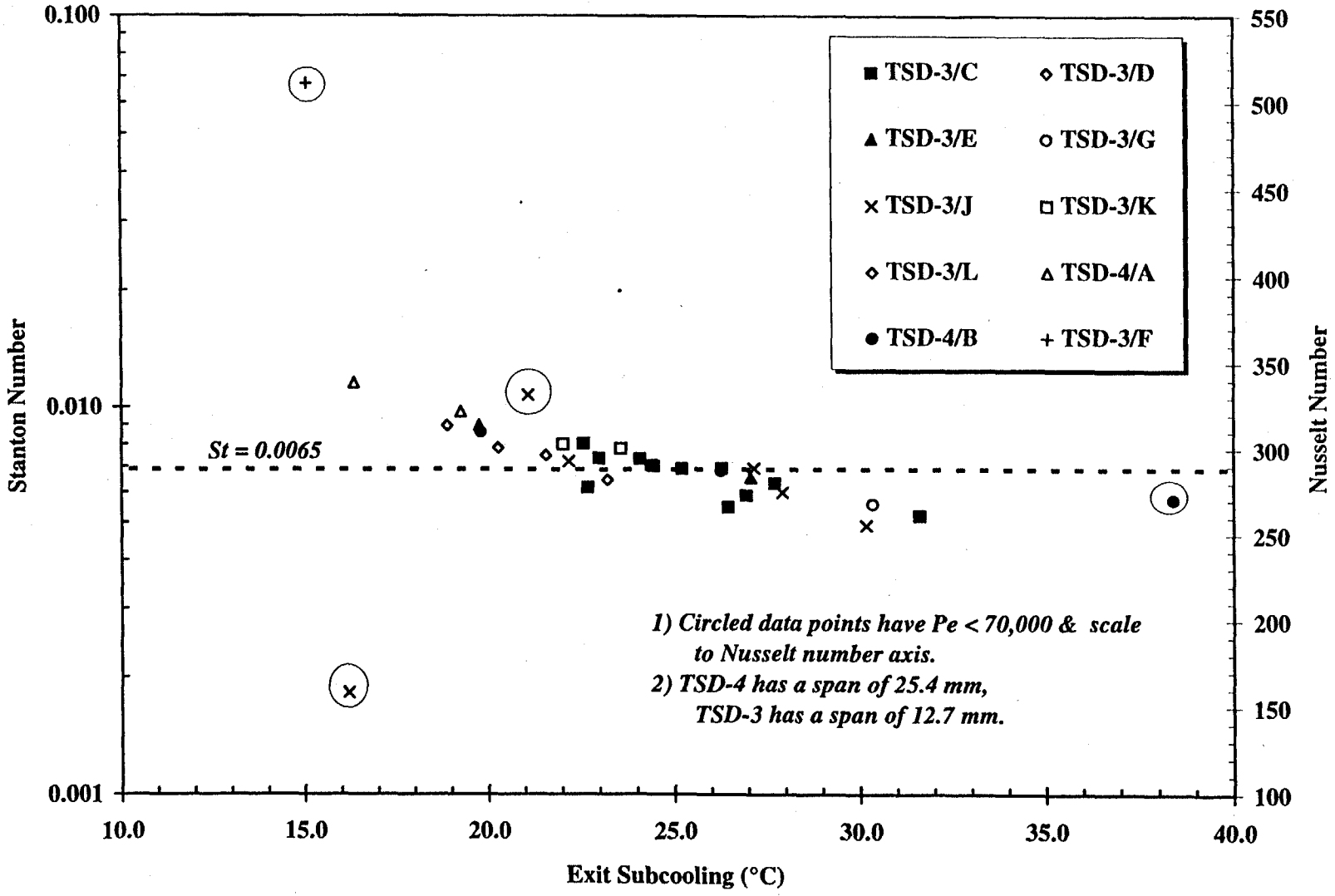

Fig. 26. Dependence of critical *St* numbers on subcooling.

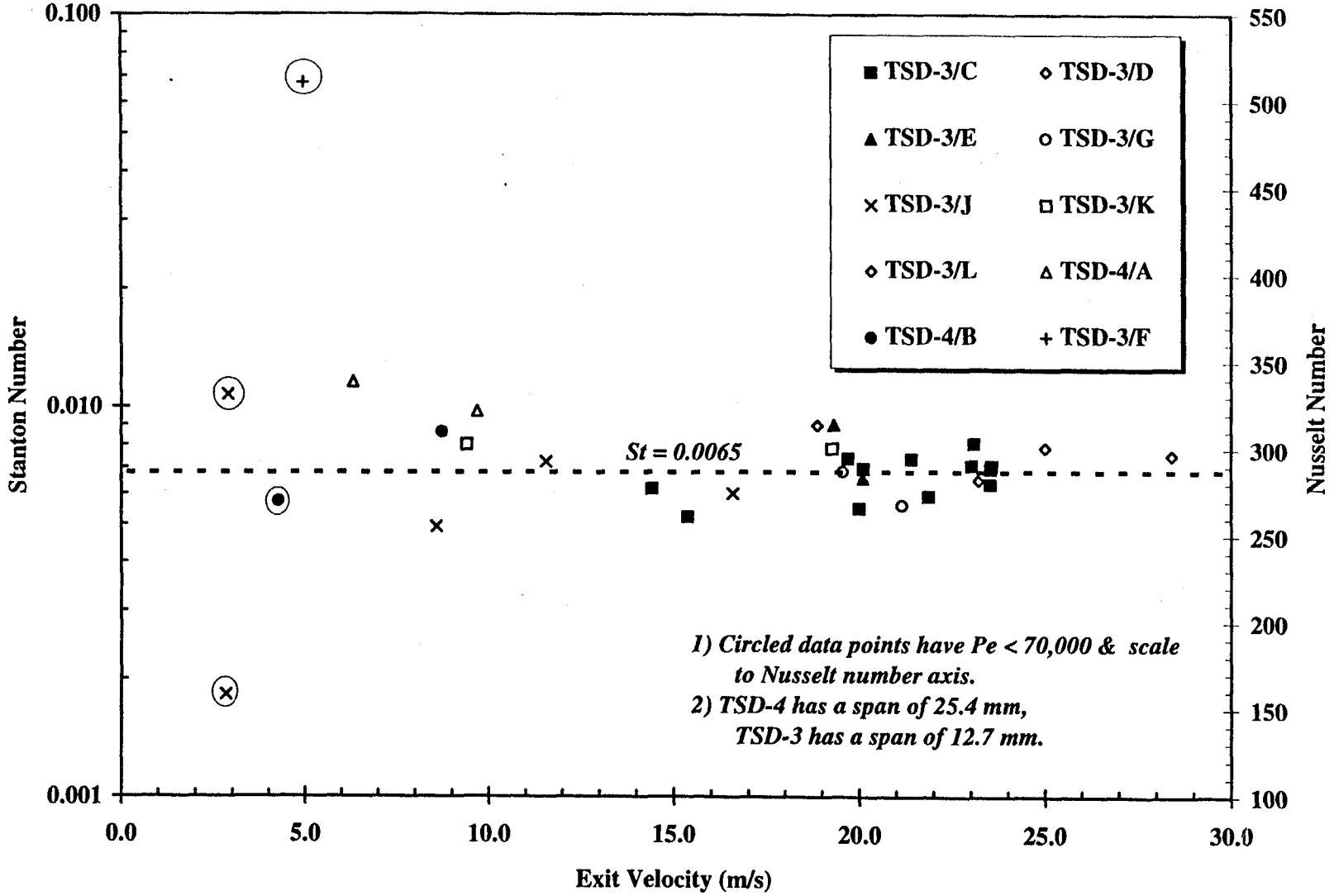

Fig. 27. Dependence of critical *St* numbers on velocity.

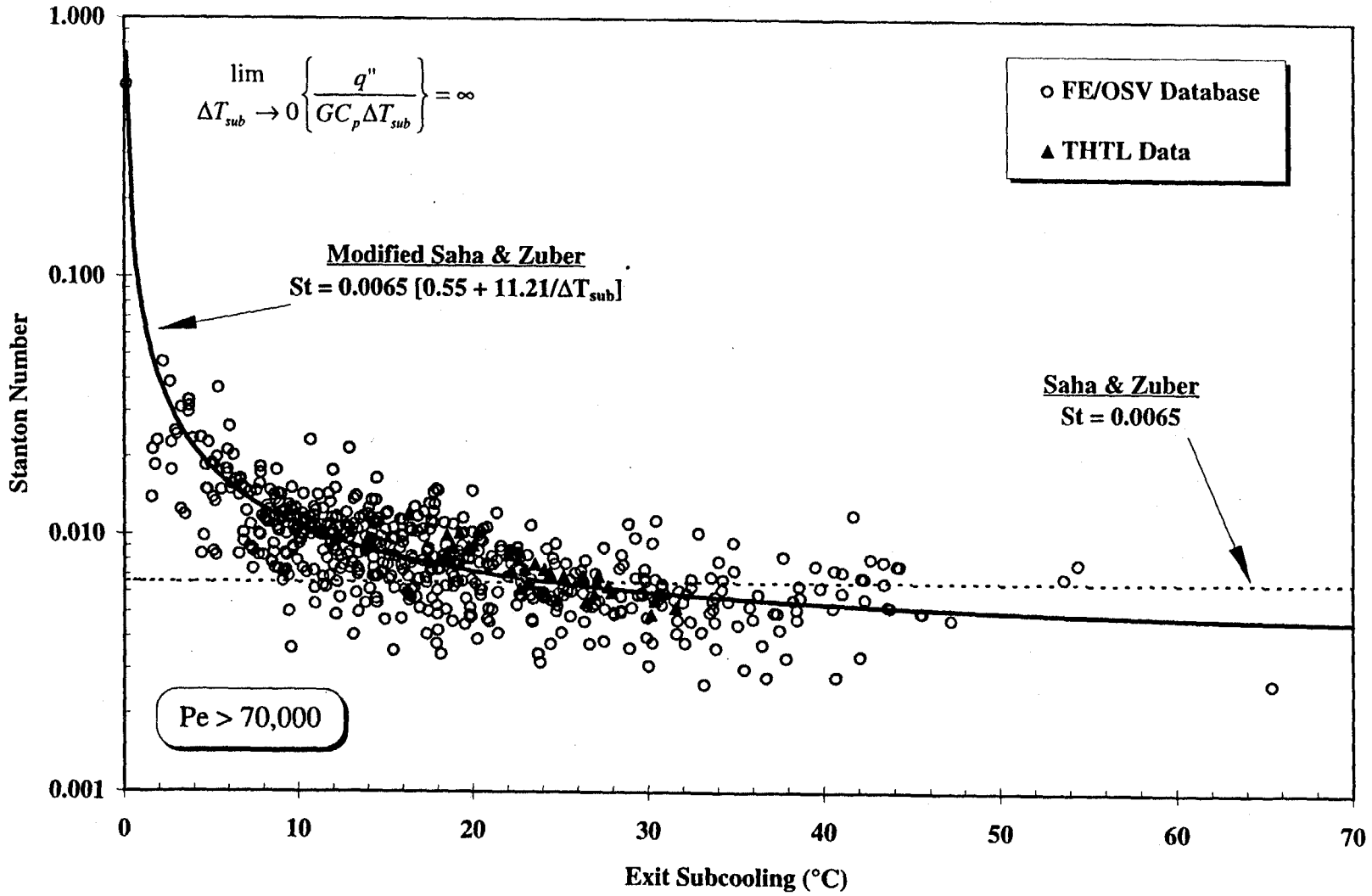

Fig. 28. Data comparison of proposed modified Saha and Zuber correlation for Stanton number.

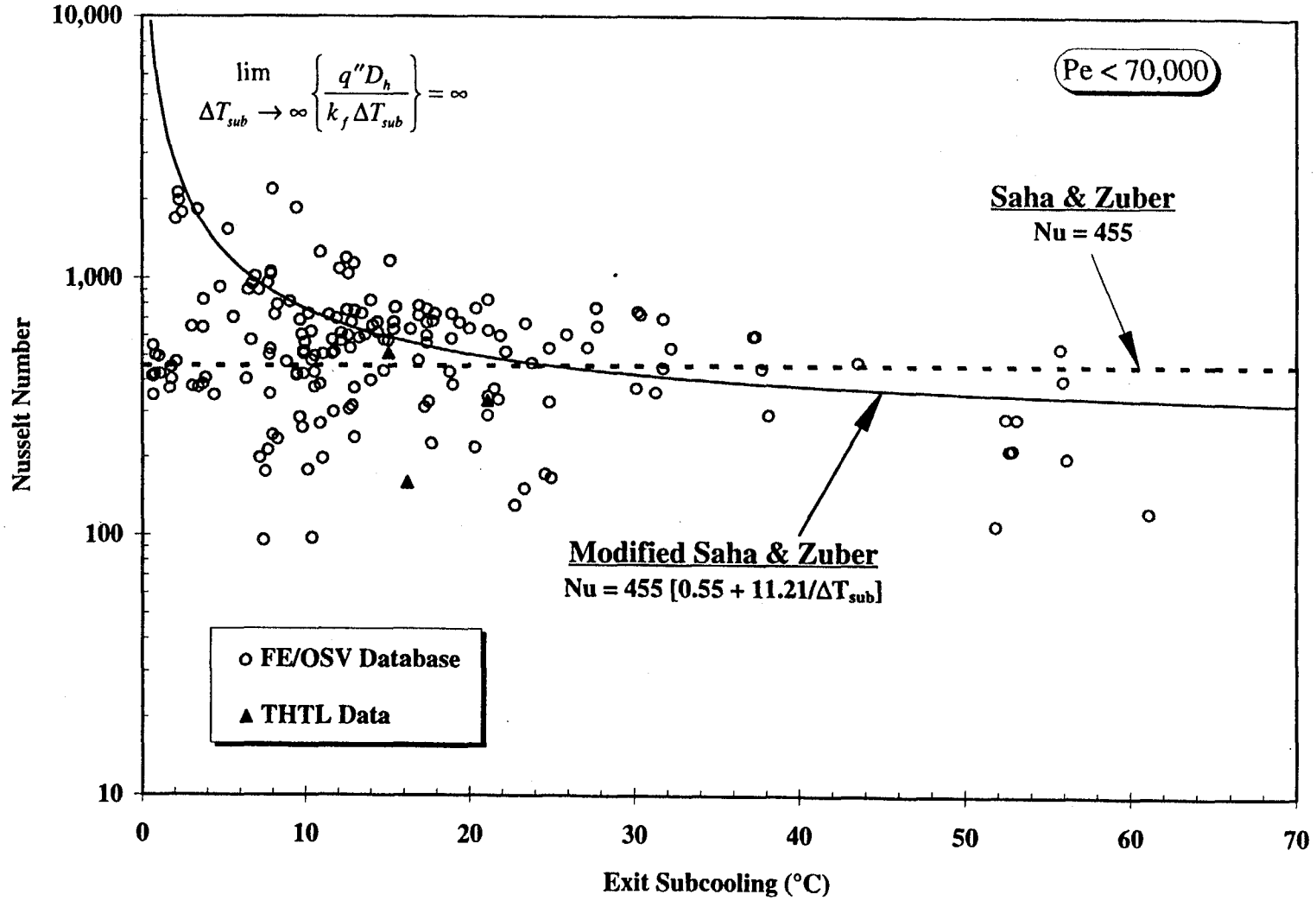

Fig. 29. Data comparison of proposed modified Saha and Zuber correlation for Nusselt number.

The following comments should be noted concerning the proposed modification.

1. As seen in Table 3, the modified S&Z correlation provides considerable improvement in the uncertainties compared with either the original S&Z correlation (especially at low subcooling) or the Costa correlation (especially at high velocities). The mean and standard deviation in *St* numbers were 1.07 and 22%, respectively, when comparing them with the modification. Comparison with the worldwide data base showed a mean and standard deviation of 1.4 and 52%, respectively, for the original S&Z correlation and 1.02 and 30% for the modification.
2. The original S&Z correlation (using *St* and *Nu* numbers) for predicting OSV were modified based on a mixture of actual FE and OSV data. Therefore, the modified correlations here are probably more reflective of FE than of OSV.
3. There is a definite advantage for the ANSR analysis to treat the statistical uncertainties in at least two velocity zones: low velocity ($V < 8$ m/s) and high velocity ($V > 8$ m/s). The correlation uncertainties for the second zone, which includes the ANSR nominal and early transient conditions, are considerably lower than those of the first.
4. Fitting the correction factor with the data was constrained to be common to both *St* and *Nu* numbers. Emphasis was put on achieving a better fit with the *St* number, resulting in a compromise for the *Nu* number.
5. A modification to the S&Z correlation for predicting FE was proposed to account for the trend of increased *St* and *Nu* numbers with reduced subcooling and also to be consistent with the definition of these two parameters. The proposed modification provides better agreement and smaller standard deviations than either the Costa or the original S&Z correlation, based on both the THTL data and the broader ANS data base.
6. The results of the four wider span tests performed show results with a somewhat higher *St* number. However, they are not inconsistent with the rest of the data. Additional tests were planned to confirm this conclusion.
7. Although a modification to the S&Z correlation was proposed for FE prediction, final correlation of the data for FE and CHF was not fully completed.

10. SUMMARY AND CONCLUSIONS

The initial focus of the THTL experimentation for the ANSR was the determination of thermal limits under ANS nominal conditions using water as the coolant. Plans included additional experiments to be performed with the existing facility and test section design to capture the onset of IB, the single-phase heat transfer coefficients and friction factors, and the two-phase heat transfer and pressure drop characteristics.

Also under consideration were plans for off-nominal conditions experiments, including low-flow tests simulating shutdown and refueling conditions, low-pressure conditions simulating LOCA and other selected quasi-equilibrium situations encountered during transient scenarios, the effect of oxide buildup, the effects of different materials and surface roughness, and the effect of heavy water on the thermal limits (CHF, FE, and IB).

Other experiments would have required modifying the THTL facility, including adding new test section designs to accommodate additional requirements. This program included a full-span, single-sided heated channel to determine the level of lateral flow mixing in the channel and confirm the effects (or lack thereof) of channel span, a two-sided half-length heated channel to test the effects of the lateral and axial heat flux distributions, and a full-span single-sided heated channel to test the effects of hot spots and hot streaks on the CHF and FE thermal limits, respectively.

The ANS Project was closed at the end of FY 1995, and many of the plans were not implemented. However, the following intermediate conclusions could be derived from what was implemented so far.

1. A THTL facility was constructed with special consideration to ensure the capability to operate the loop in three different modes—stiff for CHF tests, modified stiff for nondestructive FE tests (detected by a minimum in pressure drop), and soft for actual FE burnout tests to most accurately simulate the multiple parallel channel configuration of the ANSR. The THTL includes a bypass line in parallel to the test section; a large, nearly positive displacement pump providing almost constant mass flux; a reduced piping volume upstream of the test section; and a significant pressure drop across the flow control valve upstream of the test section.
2. Although the experiments performed so far are in their initial stages, preliminary conclusions were derived by comparing the data to three well-known FE correlations: Costa (1967), Whittle and Forgan (1967), and Saha and Zuber (1974). All three correlations seem to be generally conservative when compared with the data, with the best agreement occurring with the S&Z correlation. The FE heat flux dependence on velocity seems to be somewhere between the 0.5 power (Costa) and 1.0 (S&Z and W&F), lying nearly in the 0.8–0.9 range proposed by the more recent correlations of Lee and Bankoff (1992) and Rogers and Li (1992).
3. Acquiring FE data at this level of heat flux and velocity is of great significance for numerous reasons. Most of the available FE data is in the low-velocity (<10 m/s) range. The data reported in this report are beyond any previously available, except those reported by Waters (1966) in support of the Advanced Test Reactor. The heat flux achieved (18 MW/m^2 at the exit) is well beyond the ANSR nominal peak heat flux of 12 MW/m^2 and almost as high as the ANSR hot channel peaking factor heat flux (peak heat flux with uncertainties). The true CHF (or the subsequent expected burnout) was not encountered before the minimum pressure drop (FE) point in any of the experiments performed thus far. Furthermore, three true CHF experiments showed a 30% to 40% margin compared to corresponding FE critical velocity and a 50% margin compared to the ANSR nominal velocity. On a preliminary basis, this result implies the existence of a good safety margin in the ANSR operating velocity for both thermal limits.
4. Some difficulties were encountered in temperature measurement, oxide layer buildup, and 3-D heat redistribution that complicated the data reduction and analysis. Those difficulties were taken into account during the data reduction process.
5. A modification to the S&Z correlation for predicting FE was proposed to account for the trend of increased *St* and *Nu* numbers with reduced subcooling and also to be consistent with the definition of these two

parameters. The proposed modification provides better agreement and smaller standard deviations than either the Costa or the original S&Z correlation, based on both the THTL data and the broader ANS data base.

6. The results of the four wider span tests performed show results with a somewhat higher *St* number. However, they are not inconsistent with the rest of the data. Additional tests were planned to confirm this conclusion.
7. Although a modification to the S&Z correlation was proposed for FE prediction, final correlation of the data for FE and CHF was not fully completed.

REFERENCES

Bergles, A. E., and Rohsenow, W. M. 1964. "The Determination of Forced Convection Surface-Boiling Heat Transfer," *ASME J. of Heat Transfer* **86**, 365–72.

Boyd, R. D. January 1985. "Subcooled Flow Boiling Critical Heat Flux (CHF) and Its Application to Fusion Energy Components. Part I: Fundamentals of CHF, and Part II: A Review of Microconvective, Experimental, and Correlational Aspects," *Fusion Tech.* **7**, 1.

Boyd, R. D. January 1988. "Subcooled Water Flow Boiling Experiments Under Uniform High Flux Conditions," *Fusion Tech.* **13**, 131–42.

Boyd, R. D. November 1989. "Subcooled Water Flow Boiling at 1.66 MPa Under Uniform High Heat Flux Conditions," *Fusion Tech.* **16**, 324.

Costa, J. 1967. *Measurement of the Momentum Pressure Drop and Study of the Appearance of Vapor and Change in the Void Fraction in Subcooled Boiling at Low Pressure*, ORNL/TR-90/21, Union Carbide Corp., Oak Ridge Natl. Lab.

Costa, J. et al. 1967. *Flow Redistribution in Research Reactors,* ORNL/TR-90/13, Union Carbide Corp., Oak Ridge Natl. Lab.

Croft, M. W. 1964. *Advanced Test Reactor Burnout Heat Transfer Test*, ATR-FE-102, Babcock & Wilcox.

Dormer, T., and Bergles, R. D. September 1964. *Pressure Drop With Surface Boiling in Small Diameter Tubes*, DSR Report No. 8767-31 (MIT-8767-31), Department of Mechanical Engineering, Massachusetts Institute of Technology.

Dougherty, T. et al. December 1989. "Flow Instability in Vertical Down-Flow at High Fluxes," ASME HTD-Vol. 119, Winter Annual Meeting, San Francisco, Calif.

Duffey, R. B., and Hughes, E. D. November 1990. "Static Flow Instability Onset in Tubes, Channels, Annuli, and Rod Bundles," ASME HTD-Vol. 150, Winter Annual Meeting, Dallas, Tex.

Felde, D. K., Yoder, G. L., and Skrzycke, D. May 1992. "The Advanced Neutron Source Thermal Hydraulic Test Loop," presented at 8th Power Plant Dynamics, Control and Testing Symposium, Knoxville, Tenn.

Felde, D. K. et al. February 1994. *ANS Thermal-Hydraulic Test Loop Facility Description,* ORNL/TM-12397, Martin Marietta Energy Systems, Inc., Oak Ridge Natl. Lab.

Filonenko, G. K. 1954. "Hydraulic Resistance in Pipes (in Russian)," *Teploenergeaka* **1**(4), 4044.

Gambill, W. R. 1963. "Generalized Prediction of Burnout Heat Flux for Flowing, Subcooled, Wetting Liquids," *Chem. Eng. Prog. Symp. Series* **59**(41), 71–87.

Gambill, W. R., and Bundy, R. D. 1964. "Heat Transfer Studies of Water Flow in Thin Rectangular Channels, Part I: Heat Transfer, Burnout, and Friction for Water in Turbulent Forced Convection," *Nucl. Science and Eng.* **18**, 69–79.

Johnston, B. S. 1988. *Subcooled Boiling of Downward Flow in a Vertical Annulus,* DPST-88-891, Savannah River Laboratory.

Lafay, J., Maisonnier, G., and Girard, F. 1965. *Compte rendu d'essais flux de redistribution de debitexpulsion et calefactiona basse pression et qux faibles bitesses en canal rectangulaire*, TT/65-17-B/JL-GM-FG.

Leddineg, M. 1938. "Unstabitit der Stromung bei naturlichen und Zwangumlauf," *die Warme* **61**(48), 891–98.

Leddineg, M. 1949. "Flow Distribution in Forced-Circulation Boilers," *The Engineering Digest* **10**, 85–89.

Lee, S. C., Doria, H., and Bankoff, S. G. 1992. "A Critical Review of Predictive Models for the Onset of Significant Void in Forced-Convection Subcooled Boiling," ASME HT-Vol. 217, Winter Annual Meeting, Anaheim, Calif.

Lee, S. C., and Bankoff, S. G. August 1992. "Prediction of the Onset of Significant Void in Down Flow Subcooled Nucleate Boiling," ASME HTD-Vol. 197, *Proceedings of the 28th National Heal Transfer Conference and Exhibition,* San Diego, Calif.

Maulbetsch, J. S., and Griffith, P. April 1965. "A Study of System-Induced Instabilities in Forced-Convection Flows With Subcooled Boiling," Report No. 5382–35, Massachusetts Institute of Technology, Department of Mechanical Engineering.

Petukhov, B. S. 1970. "Heat Transfer and Friction in Turbulent Pipe Flow with Variable Physical Properties," *Advances in Heat Trans.* **6**, 528.

Rogers, J. T., and Li, J. November 1992. "Prediction of the Onset of Significant Void in Flow Boiling of Water," ASME HTD-Vol. 217, Winter Annual Meeting, Anaheim, Calif.

Saha, P., and Zuber, N. 1974. "Point of Net Vapor Generation and Vapor Void Fraction in Subcooled Boiling," *Proceedings of the 5th International Heat Transfer Conference,* Tokyo, **IV**, 175–79.

Siman-Tov, M. et al. December 1991. "Thermal-Hydraulic Correlations for the Advanced Neutron Source Reactor Fuel Element Design and Analysis," ASME HTD-Vol. 190, Winter Annual Meeting, Atlanta, Ga.

Siman-Tov, M. et al. August 1993. "Experimental Investigation of Thermal Limits in Parallel Plate Configuration for the Advanced Neutron Source Reactor," AIChE Vol. 89, pp. 86–97, 29th National Heat Transfer Conference, Atlanta, Ga.

Siman-Tov, M. et al. 1996. "Thermal-Hydraulic Correlations and Experimental Database for the Advanced Neutron Source Reactor-Closing Report," ORNL/TM-13081, Lockheed Martin Energy Systems, Inc., Oak Ridge Natl. Lab.

Siman-Tov, M. et al. March 1995. "Experimental Study of Static Flow Instability in Subcooled Flow Boiling in Parallel Channels," 4th ASME/JSME Thermal Engineering Joint Conference, Hawaii.

Siman-Tov, M. et al. April 1995. "Static Flow Instability in Subcooled Flow Boiling in Parallel Channels," 2d International Conference on Multiphase Flow '95, Kyoto, Japan.

Siman-Tov, M. et al. 1994. *FY 1993 Progress Report on the ANS Thermal-Hydraulic Test Loop Operation and Results,* ORNL/M-3789, Martin Marietta Energy Systems, Inc., Oak Ridge Natl. Lab.

Waters, E. D. May 1966. "Heat Transfer Experiments for Advanced Test Reactor," BNWL-216, Battelle Northwest Laboratory.

Weatherhead, R. J. March 1963. "Nucleate Boiling Characteristics and the Critical Heat Flux Occurrence in Subcooled Axial-Flow Water Systems," ANL-6675, Argonne National Laboratory.

Whittle, R. H., and Forgan, R. 1967. "A Correlation for the Minima in the Pressure Drop vs Flow-Rate Curves for Sub-Cooled Water Flowing in Narrow Heated Channels," *Nuclear Eng. and Design* **6**, 89–99.

Yan, H., and Theofanous, T. G. January 1992. "Thermal Mixing in the ANS Core Channels," Study for Oak Ridge National Laboratory, University of California, Santa Barbara.

Yoder, G. L et al. 1993. *Steady-State Thermal-Hydraulic Design Analysis of the Advanced Neutron Source Reactor,* ORNL/TM-12398, Martin Marietta Energy Systems, Inc., Oak Ridge Natl. Lab.

Appendix A

THTL Data Deduction and Analysis Model

(J. L. McDuffee)

Table A.1. Measured Data List and Description

Variable Name	Array Elements	Measured / Calculated	Description
RecordTime	1	M	time that the data set was taken (hh:mm:ss)
TT(101 To 118)	18	M	external wall temperature (°C)
TE119	1	M	lower aluminum bus temperature (°C)
TE120	1	M	upper aluminum bus temperature (°C)
TE121	1	M	upper aluminum bus temperature (°C)
TE202C	1	M	pump suction temperature (°C)
TE500	1	M	letdown line temperature (°C)
TE201A	1	M	bulk fluid inlet temperature (°C)
TE202A	1	M	bulk fluid exit temperature (°C)
TE201B	1	M	bulk fluid inlet temperature (°C)
TE202B	1	M	bulk fluid exit temperature (°C)
PT202	1	M	exit pressure (MPa)
BypassRatio	1	M	bypass ratio (--)
PDT101	1	M	inlet to exit differential pressure (MPa)
PT200	1	M	pump suction pressure (MPa)
PT500	1	M	test section inlet pressure (MPa)
Velocity	1	C	inlet coolant velocity (m/s)
FT201	1	M	inlet volumetric flow rate (l/s)
FT202	1	M	bypass inlet volumetric flow rate (l/s)
AT400	1	M	pH (--)
CT400	1	M	coolant electrical conductivity (μS/m)
TSPower	1	C	calculated test section power (kW)
PT203	1	M	test section exit pressure (MPa)
IE101A	1	M	current for power supply #1 (A)
PumpSpeed	1	M	pump speed (%)
IE101B	1	M	current for power supply #2 (A)
FCVposition	1	M	flow control valve position (% closed)
EE101	1	M	test section voltage drop (V)
qflux	1	C	average heat flux (MW/m^2)
TT130	1	M	top flange temperature (°C)
TT131	1	M	bottom flange temperature (°C)
JT101A	1	M	calculated power (kW)
ET(201 To 210)	10	M	local voltage drop (V)
Vtotal	1	C	sum of local voltage drop (V)
Empty(60 To 65)	6	--	future expansion slots

Table A.2. Variable Definitions Used In the THTL Data Reduction Program.

Name	Description
	PointID: Data Set Identification
Date	test date
Case * 3	test case and number, e.g. "A01," "B11," etc.
PRNfile * 11	name of file that holds measured data, e.g. "FE32494.prn"
MaxPoints(1 To 6)	number of selected data points for up to six cases
DataPosition(6, 30)	record numbers for each selected data point for up to six cases
TSD_Name * 3	test section name, e.g. "3/C"
TSD_Num	test section number
	Measured: Interpreted Measured Data
Tin	inlet bulk temperature (°C)
Texit	exit bulk temperature (°C)
Teast(1 To 9)	east side external wall temperature (°C)
Twest(1 To 9)	west side external wall temperature (°C)
Pin	inlet pressure (Pa)
Pexit	exit pressure (Pa)
dP	test section pressure drop (Pa)
G	total mass flux (kg/m^2s)
TotalPower	total test section power (W)
Amps	test section current (A)
Voltage	test section voltage drop (V)
Volts(1 To 9)	local voltage drop (V)
Power(1 To 9)	local power (W)
	Options: user options
InletTemp	inlet temperature is TE202A, TE202B, or average
ExitTemp	exit temperature is TE202A, TE202B, or average
qMethod	local heat flux based on local voltage measurements or aluminum resistivity
PowerSource	describes whether one or two power sources are used
PowerRun	if true then test is a powered run
SumVolts	if true then the sum of local voltage drops is used for total voltage drop
INele	number of axial elements
AutoLossSC	if true then heat redistribution is automatically estimated
AutoOxide	if true then oxide thickness is automatically estimated
AutoHtLoss	if true then heat losses are automatically estimated
SpecialX	x-coordinate used in transient graphics
SpecialY	y-coordinate used in transient graphics
Predictor	if true then Predictor capability is on
CritPt	thermocouple number where critical point is expected
FreeVar	designates the variable changed during a prediction sequence for a critical point
CritVar	IB, FE, or CHF
	TS: overall test section quantities
Locat(1 To 9)	thermocouple location (m)
Lele(1 To 9)	length of an axial segment (m)

Name	Description
thal	thickness of the aluminum wall in the flats (m)
xa	thickness of the aluminum in the semi-circular section (m)
xb	rectangular extension region distance in semi-circular section (m)
gap	test section gap (m)
span	test section span in the rectangular section (n_
Acs	cross sectional area aluminum test section walls (m^2)
L	test section length (m)
FlowRatio	mass flux in rectangular channel / average mass flux
Koxide	oxide conductivity (W/m°C)
INele	number of axial segments
Heater: test section heater characteristics	
tspwr	power delivered to the coolant (W)
Power(1 To 9)	local power delivered to the coolant (W)
TotalLoss	total heat loss / total applied power
TotalLossSC	heat redistribution / total applied power
Floss(1 To 9)	nonuniform heat loss function
Loss(1 To 9)	local heat loss
LossSC(1 To 9)	local heat redistribution to semi-circular channel
Oxide(1 To 9)	local oxide thickness (m)
Tmeas(1 To 9)	local measured outside wall temperature (°C)
Tpred(1 To 9)	local predicted outside wall temperature (°C)
Tav(1 To 9)	average aluminum temperature (°C)
Talox(1 To 9)	aluminum / oxide interface temperature (°C)
Twallm(1 To 9)	inside wall temperature based on external wall temperature (°C)
Twallp(1 To 9)	inside wall temperature based on bulk coolant temperature (°C)
HTCp(1 To 9)	predicted heat transfer coefficient (W/m^2 °C)
HTCm(1 To 9)	measured heat transfer coefficient (W/m^2 °C)
Section: local quantities for rectangular, semi-circular, and average channel	
qflux(1 To 10)	local heat flux (W/m^2)
Pout(0 To 10)	exit axial segment pressure (Pa)
Ptc(0 To 10)	pressure at the thermocouple location (Pa)
Pexit	test section exit pressure (Pa)
G	mass flux (kg/m^2s)
Tbulk(0 To 10)	bulk temperature at thermocouple location(°C)
Tout(0 To 10)	segment exit bulk temperature (°C)
Stanton(0 To 10)	local Stanton number (--)
qFEsz(0 To 10)	flow excursion heat flux based on Saha & Zuber correlation (W/m^2)
qFEmsz(0 To 10)	flow excursion heat flux based on Modified Saha & Zuber correlation (W/m^2)
qIB(0 To 10)	incipient boiling heat flux based on Bergles & Rohsenow correlation (W/m^2)
qCHF(0 To 10)	critical heat flux based on Gambill / Weatherhead correlation (W/m^2)
Dh	hydraulic or equivalent diameter (m)
Peri	heated perimeter (m)
Aflow	bulk flow area (m^2)

INTERNAL DISTRIBUTION

1. J. H. Campbell
2. J. J. Carbajo
3. N. C. J. Chen
4. D. H. Cook
5. J. A. Crabtree
6. W. G. Craddick
7. J. R. Dixon
8. G. Farquharson
9. E.C. Fox
10. J. D. Freels
11. G. E. Giles
12. R. M. Harrington
13. J. A. March-Leuba
14. M. T. McFee
15. D. G. Morris
16. R. E. Rothrock
17. D. L. Selby
18–22. M. Siman-Tov
23. M. W. Wendel
24. C. D. West
25. G. L. Yoder
26–27. Central Research Library
28. Y-12 Technical Library
29. Laboratory Records Dept.
30-31. Laboratory Records (RC)

EXTERNAL DISTRIBUTION

32. Ronald Boyd, Prairie View A&M University, P.O. Box 397, Prairie View, TX 77446
33. L. Y. Cheng, Brookhaven National Laboratory, Associated Universities, Inc., Building 120 Reactor Division, Upton, Long Island, NY 11973
34. Yousri Elkassabgi, Texas A&I University, Department of Mechanical Engineering, Campus Box 191, Kingsville, TX 78363
35. D. K. Felde, M4 Environmental, 1000 Clear View Court, Oak Ridge, TN 37830
36. W. R. Gambill, Route 5, Box 220, Clinton, TN 37716
37. Peter Griffith, Professor, Massachusetts Institute of Technology, Department of Mechanical Engineering, 77 Massachusetts Avenue, Room 7 044, Cambridge, MA 02139
38. M. Kaminaga, Tokai Research Establishment, Japan Atomic Energy Research Institute, Todai-mura, Naka-gun, Ibaraki-ken, 319-11, JAPAN
39. A. E. Ruggles, Pasqua Nuclear Engineering Building, University of Tennessee, Knoxville,TN 37996-2300
40. T. G. Theofanous, 857 Sea Ranch Drive, Santa Barbara, CA 93109
41. G. E. Wilson, EG&G Idaho, Inc., P.O. Box 1625 (MS-3895), Idaho Falls, ID 83415-3895
42. Wolfgang Wulff, Brookhaven National Laboratory, Associated Universities, Inc., Upton, NY 11973

43–44. Office of Scientific and Technical Information, P. O. Box 62, Oak Ridge, TN 37831